E. Wolf, Progress in Optics 51

Chapter 1

Negative refractive index metamaterials in optics

by

Natalia M. Litchinitser

Department of Electrical Engineering and Computer Science, University of Michigan, 2200 Bonisteel Boulevard, 3113 ERB1, Ann Arbor, Michigan 48109, USA
e-mail: natashan@eecs.umich.edu

Ildar R. Gabitov

Department of Mathematics, University of Arizona, 617 North Santa Rita Avenue, Tucson, Arizona 85721, USA

Andrei I. Maimistov

Department of Solid State Physics, Moscow Engineering Physics Institute, Kashirskoe sh. 31, Moscow 115409, Russian Federation

Vladimir M. Shalaev

School of Electrical and Computer Engineering and Birck Nanotechnology Center, Purdue University, West Lafayette, Indiana 47907, USA

ISSN: 0079-6638 DOI: 10.1016/S0079-6638(07)51001-2

Contents

§ 1. Introduction

Recent advances in nanofabrication have led to the demonstration of a novel class of optical materials – metamaterials – that are artificially engineered structures with electromagnetic properties unattainable in nature. One of the most fascinating examples of such structures is negative-index metamaterials (NIMs). The emergence of optical metamaterials opens up fundamentally new regimes of light–matter interaction and prompts unique opportunities for manipulating light.

Over the last seven years there has been enormous progress in the field of NIMs from both theoretical and experimental viewpoints (Ramakrishna [2005], Veselago, Braginsky, Shklover and Hafner [2006]). The latest developments in the field of negative refraction and microwave/terahertz NIMs have been reviewed by Pendry [2004], Smith, Pendry and Wiltshire [2004], Boardman, King and Velasco [2005] and others. Recent advancements in the studies of highly unusual linear properties of optical NIMs have been discussed by Veselago and Narimanov [2006], Agranovich and Gartstein [2006], and Klar, Kildishev, Drachev and Shalaev [2006]. Some remarkable nonlinear properties of NIMs have been highlighted in the recent *Nature Photonics* article by Shalaev [2007]. In this review we intend to present a comprehensive overview of the state of the art in the design and fabrication of NIMs at optical frequencies, their linear and nonlinear properties, and potential applications of optical NIMs and a more general class of optical metamaterials.

1.1. Ambidextrous light in a left-handed world

The propagation of electromagnetic waves in optical media is determined by two material parameters: dielectric permittivity ε and magnetic permeability μ, related to the refractive index n through $n = \sqrt{\varepsilon\mu}$. Figure 1a shows a diagram of all possible combinations of ε and μ. The majority of conventional materials belongs to region I where $\varepsilon > 0$ and $\mu > 0$ corresponding to $n > 0$, where propagating waves are allowed. It is noteworthy that the magnetic susceptibility of most natural materials is very small in comparison with their dielectric sus-

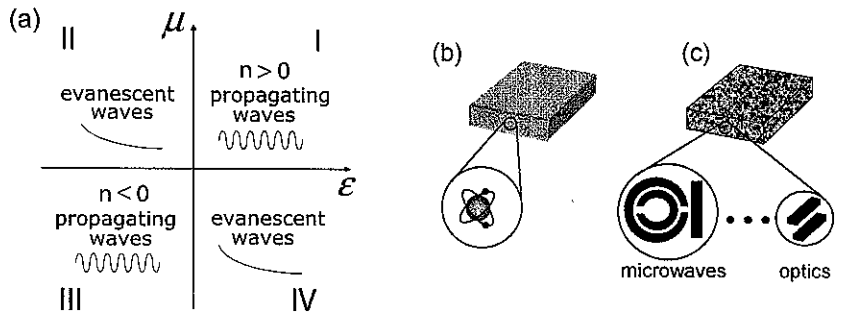

Fig. 1. (a) A diagram of all possible combinations of dielectric permittivity ε and magnetic permeability μ. (b) A conventional material built of regular atoms. (c) A metamaterial built of "meta-atoms".

ceptibility, thus limiting the interaction of atoms to the electric component of the electromagnetic wave, leaving the magnetic component largely unexploited. Indeed, μ is close to unity for many naturally existing materials. The reason for this difference in the strength of electric and magnetic field coupling to atoms is that the magnetization of any (non-ferromagnetic) material is a relativistic effect, of the order $\sim v^2/c^2 \sim \alpha^2 \ll 1$, where v is the velocity of the electrons in the atoms, and $\alpha \cong 1/137$ is the fine-structure constant (Landau, Lifshitz and Pitaevskii [1984]). Magnetism is particularly weak at optical frequencies because the relaxation times of paramagnetic and ferromagnetic processes are significantly longer than the optical period, leaving the electron movement in atoms as the only mechanism for the magnetic response. As a result, the magnetic field component is usually not involved in light–matter interactions. Only at very high intensities of $\sim 10^{18}$ W/cm^2 do the effects of the magnetic and electric fields on the electron motion become comparable, giving rise to a number of new effects such as the photon-drag effect (Wegener [2005]) and nonlinear Thomson scattering or Larmor radiation (Wegener [2005], Chen, Maksimchuk and Umstadter [1998]).

The second ($\varepsilon < 0$ and $\mu > 0$) and fourth ($\varepsilon > 0$ and $\mu < 0$) quarters of the diagram in fig. 1 correspond to opaque materials that cannot support any propagating waves. However, materials with parameters corresponding to the third quarter of the diagram ($\varepsilon < 0$ and $\mu < 0$) are transparent and allow wave propagation. While the dielectric permittivity of some naturally occurring materials is negative in certain frequency ranges (e.g. metals including gold, silver and aluminum possess negative ε at the visible and near-ultraviolet frequencies), no isotropic materials with negative μ are readily available. Some antiferromagnets and insulating ferromagnets have been shown to provide negative effective magnetic permeability (Campley and Mills [1982], Hartstein, Burstein, Maradudin, Brewer

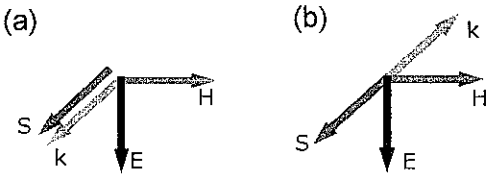

Fig. 2. (a) Vectors E, H, and k form a "right-handed" triplet in PIMs, and (b) a "left-handed" triplet in NIMs.

and Wallis [1973]). Moreover, the possibility of simultaneously realizing negative effective ε_{eff} and μ_{eff} in antiferromagnetic metals has been discussed by Campley and Mills [1982]. Nevertheless, no materials with ε and μ being simultaneously negative had been found in nature or demonstrated experimentally prior to the year 2000. But what is so exciting about such materials?

In 1968, Veselago showed theoretically that materials with simultaneously negative ε and μ possess a number of unusual and often counterintuitive properties. To understand a lightwave interaction with such materials, let us consider Maxwell's equations written in the form

$$k \times E = \frac{\omega}{c}\mu H,$$
$$k \times H = -\frac{\omega}{c}\varepsilon E. \tag{1.1}$$

Equations (1.1) suggest that if $\varepsilon > 0$ and $\mu > 0$ in the same frequency range, the vectors E, H and k form a "right-handed" triplet as shown in fig. 2a, and the refractive index is positive. As usual, the Poynting vector, defined as

$$S = \frac{c}{4\pi} E \times H, \tag{1.2}$$

is parallel to the k-vector. However, if $\varepsilon < 0$ and $\mu < 0$ in the same frequency range, the vectors E, H and k form a "left-handed" triplet as shown in fig. 2b, and the refractive index is negative, i.e. $n = -\sqrt{\varepsilon\mu}$. The former class of materials is often referred to as "right-handed materials" (RHMs) or positive-index materials (PIMs), while the latter class is referred to as "left-handed materials" (LHMs) or negative-index materials (NIMs). The Poynting vector in NIMs is anti-parallel to the k-vector. Therefore, the phase velocity, defined as $v_{\text{p}} = \omega/k$, is co-directed with the energy velocity determined by the Poynting vector in PIMs and counter-directed with the Poynting vector in NIMs. The opposite directionality of the phase velocity and the Poynting vector is taken as the most general definition of NIMs.

Although the LHMs introduced by Veselago have been assumed to have ε, μ and n negative (and real) numbers in the same frequency range, the term "left-handed materials" is often used in a broader context to include other optical systems that possess antiparallel phase velocity and the Poynting vector. Examples of such materials, including photonic crystals, anisotropic waveguides, and others, will be discussed in § 2.

We note that there are two general theoretical approaches to the description of NIMs at optical frequencies. In one approach [used in eq. (1.1)] a set of four fields, E, D, H, and B, is introduced, where $D = \varepsilon(\omega)E$, $B = \mu(\omega)H$ for a monochromatic wave. In another approach the so-called E,B&D picture is used, in which $B = H$, with $\mu = 1$, and $D = \varepsilon E$ with $\varepsilon = \varepsilon(\omega, k)$, including both temporal and spatial dispersions (Agranovich, Shen, Baughman and Zakhidov [2004a]). There is, however, a one-to-one correspondence in the formal description of propagation in NIMs by the two approaches. In this chapter the (E, D, H, B) approach will be followed.

As mentioned above, a negative refractive index has not been found in naturally occurring materials due to the limitations imposed on their properties by their constituent components – atoms and molecules schematically shown in fig. 1b. On the contrary, metamaterials are built of so-called artificial or "meta"-atoms (fig. 1c). Meta-atoms are properly engineered resonant nanostructures that bring new degrees of freedom to the design of functional materials. The electrical permittivity and magnetic permeability of metamaterials can, in principle, be designed positive, negative or even zero at any selected frequency by properly adjusting the dimensions, periodicity and other properties of the meta-atoms. Therefore, metamaterials can fundamentally change both linear and nonlinear light–matter interactions by bringing the magnetic component of the field into play in addition to its electric component and thus making the electromagnetic waves "ambidextrous" in the optical domain. The current state of the art in the design and fabrication of optical metamaterials will be discussed in § 2.

The nonlinear properties of metamaterials are also expected to be significantly modified by their design, and in particular by their enhanced interactions with the magnetic field component. The nonlinear response of metamaterials has been analyzed for the particular case of a two-dimensional NIM periodic structure created by arrays of wires and split-ring resonators (SRR) embedded in a nonlinear dielectric host material, and has been shown to have two different contributions (Zharov, Shadrivov and Kivshar [2003]): the first contribution originates from an intensity-dependent part of the effective dielectric permittivity of the nonlinear dielectric host material, and the second contribution comes from the periodic structures of resonators. The magnetic nonlinearity has been found to be much

stronger than the nonlinearity in the dielectric properties due to the field enhancement in the split-ring resonators, as will be discussed in more detail in § 4. Nevertheless, quoting a recent paper by Klein, Enkrich, Wegener and Linden [2006] "a systematic microscopic theory of the nonlinear optical properties of metallic metamaterials would be highly desirable but is currently not available."

Antiparallel v_p and S in NIMs have been shown to manifest in many extraordinary optical phenomena, including negative refraction and amplification of the evanescent waves, remarkably changed Manley–Rowe power conservation relations and new "backward" phase-matching conditions (Veselago [1968], Pendry [2000], Zharov, Zharova, Shadrivov and Kivshar [2005], Popov and Shalaev [2006a, 2006b], Popov, Slabko and Shalaev [2006], Shadrivov, Zharov and Kivshar [2006], Maimistov, Gabitov and Kazantseva [2007]), surface and guided-wave regimes unattainable in conventional waveguides, and new types of temporal and spatial solitons (Scalora, Syrchin, Akozbek, Poliakov, D'Aguanno, Mattiucci, Bloemer and Zheltikov [2005], Scalora, D'Aguanno, Mattiucci, Akozbek, Bloemer, Centini, Sibilia and Bertolotti [2005], Lazarides and Tsironis [2005], Kourakis and Shukla [2005], Shadrivov, Zharova, Zharov and Kivshar [2005], Shadrivov and Kivshar [2005], Gabitov, Indik, Litchinitser, Maimistov, Shalaev and Soneson [2006], Marklund, Shukla and Stenflo [2006]; these will be discussed in §§ 4–7.

Recently, several novel device applications have been proposed that rely on the negative phase shift (phase advance) introduced by NIMs. These include miniaturized optical resonators, phase compensators/conjugators, sub-wavelength waveguides, couplers, and laser cavities (Engheta [2002], Alu and Engheta [2003, 2004], Caiazzo, Maci and Engheta [2004], Engheta and Ziolkowski [2005], Ziolkowski [2006]). Negative phase shifts have been predicted to have a pronounced effect on optical bistability, potentially facilitating new tools for NIM characterization, and to enable enhanced nonreciprocal transmission that can be utilized in optical diode-like device applications (Feise, Shadrivov and Kivshar [2004, 2005], D'Aguanno, Mattiucci, Scalora and Bloemer [2004], Hegde and Winful [2005a], Jiang, Chen and Zhu [2006], Litchinitser, Gabitov, Maimistov and Shalaev [2007]). These effects and applications will be discussed in §§ 5 and 7.

Finally, in addition to the exciting phenomena and potential applications associated with NIMs per se, a more general class of metamaterials, including NIMs, has been shown to provide new ways for the manipulation of an object's degree of visibility (Alu and Engheta [2005a], Pendry, Schurig and Smith [2006], Leonhardt [2006], Leonhardt and Philbin [2006], Milton and Nicorovici [2006], Schurig, Mock, Justice, Cummer, Pendry, Starr and Smith [2006], Cai, Chettiar, Kildishev

and Shalaev [2007]). The theoretical aspects and first experimental realization of metamaterial-based cloaking will be discussed in § 8.

1.2. Negative index: Brief history

A most comprehensive theoretical description of NIMs has been presented by Veselago [1968], who formulated and analyzed the most important properties of NIMs with ε and μ being negative in the same frequency range and also addressed the issue of the practical realization of such materials. However, the possibility of opposite directionality of the phase and energy velocities has been discussed at least as early as in 1904–1905 by Lamb in his paper "On group-velocity" and by Von Laue [1905]. Lamb [1904] acknowledged Schuster for noticing that a group velocity can be negative (i.e., can have a sign opposite to that of the phase velocity) owing to anomalous dispersion. Lamb [1904] and Pocklington [1905] considered some examples of mechanical systems where the phase and group velocities can be in the opposite direction. Schuster [1904] has shown that this property could also be realized in optical systems. The first detailed discussion of negative refraction can be found in Mandelshtam's [1947] lectures, while the relationship between simultaneously negative ε and μ and negative refraction was first noted by Sivukhin [1957] and studied in more detail by Pafomov [1959]. Finally, negative refraction of a wave propagating across the boundary with a gyrotropic medium was discussed in Agranovich and Ginzburg's [1984] book.

§ 2. Optical negative index metamaterials: State of the art

The first experimental demonstrations of NIMs were reported at microwave frequencies by Smith, Padilla, Vier, Nemat-Nasser and Schultz [2000] and Shelby, Smith and Schultz [2001]. Following the approach proposed by Pendry, Holden, Robbins and Stewart [1999], these first NIMs were based on pairs of subwavelength concentric SRRs providing negative μ and straight wires responsible for negative ε. This structure can be considered as an electronic circuit consisting of inductive and capacitive elements (an LC-circuit). The rings form the inductances, while the two slits and the gap between the two rings can be considered as capacitors. A magnetic field, oriented perpendicular to the plane of the rings, induces an opposing magnetic field in the loop due to Lenz's law, which leads to a diamagnetic response resulting in a negative permeability. The capacitors are necessary to guarantee that the wavelength of the resonance is larger than the dimensions of the SRR. In this configuration, a strong magnetic response has been

achieved by operating in the vicinity of the LC resonance of the split ring (Pendry, Holden, Robbins and Stewart [1999]). The frequencies of the LC resonances in this case are largely determined by the geometry and size of the split ring rather than by the properties of the metal. At microwave frequencies, metals can be considered as perfect conductors because the skin depth is significantly smaller than the characteristic size of the meta-atom. The same technique of obtaining negative magnetic permeability using SRRs has been implemented in the terahertz frequency range by scaling down the dimensions of the split rings (Linden, Enkrich, Wegener, Zhou, Koschny and Soukoulis [2004]). However, scaling down to the near-infrared and visible frequencies turned out not to be straightforward, not only due to technical challenges related to the fabrication of resonant structures on the nanoscale, but also because metals no longer behave as perfect conductors in this frequency range and electromagnetic fields penetrate into the metal. As a result, magnetic resonance is significantly reduced. Therefore, different approaches have been developed (Shalaev, Cai, Chettiar, Yuan, Sarychev, Drachev and Kildishev [2005], Zhang, Fan, Panoiu, Malloy, Osgood and Brueck [2005], Grigorenko, Geim, Gleeson, Zhang, Firsov, Khrushchev and Petrovic [2005], Zhang, Fan, Malloy, Brueck, Panoiu and Osgood [2006], Dolling, Enkrich, Wegener, Soukoulis and Linden [2006a, 2006b], Dolling, Wegener, Soukoulis and Linden [2007]).

2.1. Plasmonic NIMs

The first metamaterials with a negative index of refraction at optical frequencies have been demonstrated using pairs of metallic nanorods by Shalaev, Cai, Chettiar, Yuan, Sarychev, Drachev and Kildishev [2005] (shown schematically in fig. 3a) and using pairs of dielectric voids in metal by Zhang, Fan, Panoiu, Malloy, Osgood and Brueck [2005] as shown in fig. 3b. In both experiments the NIMs were fabricated in the form of thin films of thicknesses 160 and 120 nm, respectively.

In such thin films Snell's law cannot be used to detect or measure the refractive index. The negative refraction property reveals itself in a phase shift (phase advance) that was measured interferometrically in the experiments (Shalaev, Cai, Chettiar, Yuan, Sarychev, Drachev and Kildishev [2005], Drachev, Cai, Chettiar, Yuan, Sarychev, Kildishev, Klimeck and Shalaev [2006], Zhang, Fan, Panoiu, Malloy, Osgood and Brueck [2005]). It is important that an unambiguous determination of the refractive index requires four parameters to be measured: transmittance T, reflectance R, and the absolute values of the phases φ_t and φ_r of the transmitted and reflected fields. Then the complex refractive index for the NIM

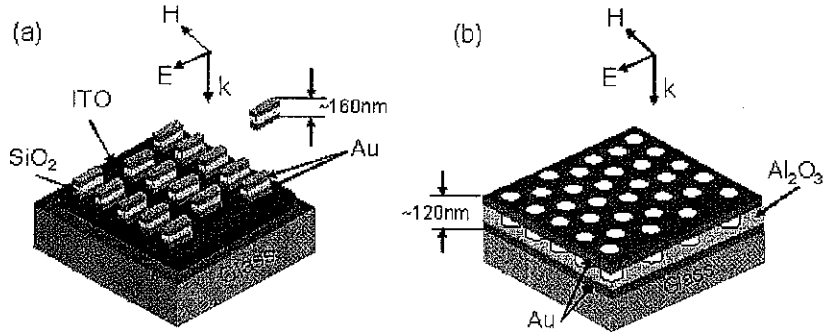

Fig. 3. Schematics of the structures fabricated and characterized in the first NIM experiments, (a) at 1.5 μm by Shalaev, Cai, Chettiar, Yuan, Sarychev, Drachev and Kildishev [2005], and (b) at 2 μm by Zhang, Fan, Panoiu, Malloy, Osgood and Brueck [2005].

thin film sandwiched between the air and glass can be found from (Kildishev, Cai, Chettiar, Yuan, Sarychev, Drachev and Shalaev [2006])

$$\cos(nk\Delta) = \frac{1 - r^2 + n_s t^2}{(n_s + 1)t + rt(n_s - 1)}, \tag{2.1}$$

where k is the wavevector of light in vacuum, Δ is the thickness of the NIM thin film, r and t are complex reflection and transmission coefficients, $t = \sqrt{T}\exp(i\varphi_t)$, $r = \sqrt{R}\exp(i\varphi_r)$, and n_s is the refractive index of the substrate.

The idea of using pairs of metallic rods to produce effective magnetic permeability was discussed for the first time by Lagarkov and Sarychev [1996]. The possibility of realizing a negative index of refraction at optical frequencies in paired nanorod composites was proposed by Podolskiy, Sarychev and Shalaev [2002] and discussed in detail by Panina, Grigorenko and Makhnovskiy [2002], Podolskiy, Sarychev and Shalaev [2003], and Podolskiy, Sarychev, Narimanov and Shalaev [2005].

The origin of a negative refractive index in a composite material built with such paired nanorods can be understood as follows. The electric resonances of an individual nanorod originate from the excitation of the surface waves on the metal–air interface. While such surface waves, known as surface plasmon polaritons, cannot be excited with the plane wave in a semi-infinite medium, they are excited in the finite size nanorods. In a paired nanorod configuration two types of plasmon polariton waves can be supported: symmetric and anti-symmetric. The electric field, oriented parallel to the nanorods, induces parallel currents (symmetric plasmon polariton wave) in both nanorods, leading to the excitation of a dipole

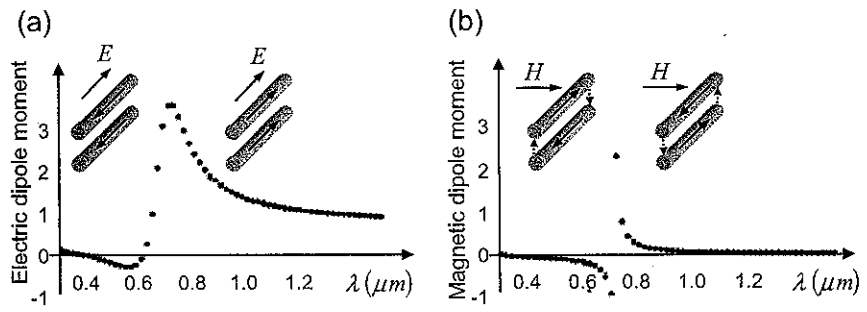

Fig. 4. (a) The electric dipole moment of a coupled nanorod pair with the length of the nanorod being $a = 162$ nm, the separation between two nanorods $d = 80$ nm, and the nanorod diameter $b = 32$ nm. (b) The magnetic dipole moment of the system in (a). (Adapted from Klar, Kildishev, Drachev and Shalaev [2006].)

moment. The magnetic field, oriented perpendicular to the plane of the nanorods, excites anti-parallel currents (anti-symmetric plasmon polariton wave) in the pair of nanorods. Combined with the displacement currents between the nanorods, they induce a resonant magnetic dipole moment. The excited moments are co-directed with the incident field when the wavelength of an incident light is above the resonance, and they are counter-directed to the incident fields at wavelengths below the resonance, as shown in fig. 4. The excitation of such plasmon resonances for both the electric and magnetic field components results in the resonant response of the refractive index. In particular, the refractive index can become negative at wavelengths below the resonance (Podolskiy, Sarychev and Shalaev [2002, 2003]).

On the other hand, the two parallel nanorods can be considered as an open current loop, which acts as a transmission line. Such a loop is closed through the displacement current, and it therefore supports the resonant modes of the electric and magnetic components of the electromagnetic field. Then, a resonance in the pair of nanorods can also be thought of as a resonance in an optical LC-circuit, with the inductance L provided by the metal rods and the capacitance C provided by the dielectric gaps between the nanorods.

While the first experiments reported by the Purdue group (Shalaev, Cai, Chettiar, Yuan, Sarychev, Drachev and Kildishev [2005]) and by the New Mexico–Columbia team (Zhang, Fan, Panoiu, Malloy, Osgood and Brueck [2005]) did prove the possibility of NIMs at optical frequencies, the first NIM samples possessed significant losses. It is noteworthy that the condition of both real ε and μ being negative, originally introduced by Veselago [1968], is a sufficient but not a necessary condition for n being negative. Indeed, Depine and Lakhtakia [2004]

have derived a more general condition that assures a negative real part of n in the form $\mathrm{Re}(\varepsilon)|\mu| + \mathrm{Re}(\mu)|\varepsilon| < 0$, assuming that $\varepsilon = \mathrm{Re}(\varepsilon) + \mathrm{i}\,\mathrm{Im}(\varepsilon)$ and $\mu = \mathrm{Re}(\mu) + \mathrm{i}\,\mathrm{Im}(\mu)$. This condition is valid for passive NIMs and suggests that a negative refractive index can be achieved even when $\mathrm{Re}(\varepsilon) < 0$ but $\mathrm{Re}(\mu) > 0$ provided that $\mathrm{Im}(\mu) \neq 0$. However, this requirement implies that the material is inherently lossy. A figure of merit (FOM) that can be used to characterize NIM performance is often defined as

$$F = \frac{|\mathrm{Re}(n)|}{\mathrm{Im}(n)}, \tag{2.2}$$

where $\mathrm{Re}(n)$ and $\mathrm{Im}(n)$ are the real and imaginary parts of n. The larger the FOM, the better the NIM's transmission properties are. However, it should be mentioned that another important factor affecting the overall transmission is impedance mismatch.

An ultimate goal of NIM design and fabrication is the demonstration of materials with a large negative real part of n, a large FOM, a broad bandwidth corresponding to both ε and μ being negative and optimized impedance matching. The current state of the art for optical NIMs was demonstrated by the Karlsruhe–Iowa State team (Dolling, Enkrich, Wegener, Soukoulis and Linden [2006a]). Using a self-supporting fishnet structure consisting of rectangular dielectric voids in parallel metal films, they achieved a FOM of 3 at $\lambda = 1.4$ μm. Recently, the Karlsruhe group has also reported the first 3-layered NIM with a FOM of 2.5 at $\lambda = 1.41$ μm.

In table 1 we summarize recent experimental results reported by different groups, and compare them in terms of $\mathrm{Re}(n)$, the operating wavelength, the FOM and the structure of the sample.

Recently, several advanced designs for optimizing NIM properties have been proposed. These include NIMs combining magnetic resonators with metal films (Chettiar, Kildishev, Klar and Shalaev [2006]), impedance-matched low-loss NIMs utilizing pairs of metal strips embedded in gain materials (Klar, Kildishev, Drachev and Shalaev [2006]), NIM structures built of periodic arrays of pairs of short metal wires and continuous wires (Zhou, Zhang, Tuttle, Koschny and Soukoulis [2006]), materials with a unit cell comprising a continuous optically thin metal film sandwiched between two identical optically thin metal strips, where the incorporation of the middle thin-metal film relaxes the requirement on large wavelength/unit cell ratios (Shvets and Urzhumov [2006], Lomakin, Fainman, Urzhumov and Shvets [2006]), metallic horseshoe-shaped or U-shaped nanostructures showing a magnetic plasmon resonance even when the characteristic size of the nanostructure is much smaller than the optical wavelength (Sarychev, Shvets and Shalaev [2006]), and finally, three-dimensional NIMs (Zhang, Fan, Panoiu, Malloy, Osgood and Brueck [2006]).

Table 1

Group	Re(n)@λ	|Re(n)|/ Im(n)	Sample
Purdue[1]	−0.3 at 1.5 μm	0.1	
New Mexico & Columbia[2]	−2 at 2 μm	0.5	
New Mexico & Columbia[3]	−4 at 1.8 μm	2	
Karlsruhe & Iowa State[4]	−1 at 1.4 μm −2 at 1.45 μm	3 1.5	
Karlsruhe & Iowa State[5]	−0.6 at 780 nm	0.5	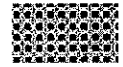
Karlsruhe[6]	−1 at 1.41 μm	2.5	 3 layers
Purdue[7]	−1 at 813 nm	1.3	

[1] Shalaev, Cai, Chettiar, Yuan, Sarychev, Drachev and Kildishev [2005].
[2] Zhang, Fan, Panoiu, Malloy, Osgood and Brueck [2005].
[3] Zhang, Fan, Malloy, Brueck, Panoiu and Osgood [2006].
[4] Dolling, Enkrich, Wegener, Soukoulis and Linden [2006a].
[5] Dolling, Wegener, Soukoulis and Linden [2007].
[6] Dolling, Wegener and Linden [2007].
[7] Chettiar, Kildishev, Yuan, Cai, Xiao, Drachev and Shalaev [2006].

2.2. *Loss management*

Among other properties, losses remain the most critical problem for the plasmonic NIMs that were fabricated and characterized in the pioneering experiments discussed in the preceding subsection. These losses are the main obstacle for the development of practical applications of optical NIMs. In particular, it has been shown that even very small losses significantly deteriorate the imaging properties of a so-called "superlens" (Podolskiy and Narimanov [2005a]).

Shamonina, Kalinin, Ringhofer and Solymar [2001] and Ramakrishna, Pendry, Wiltshire and Stewart [2003] have found that the effect of losses in bulk NIMs can be reduced by replacing a slab of bulk NIM with a layered stack of alternating NIM and PIM layers. A significant improvement can be achieved if the PIM layers are also made out of gain materials such as optically pumped semiconductors (fig. 5a) (Ramakrishna and Pendry [2003]). For example, in order to achieve a low-loss transmission in silver layers in red light, blue or ultraviolet pumped AlGaAs layers can be used as gain elements. A significant improvement in transmission has been demonstrated for the silver/gain material

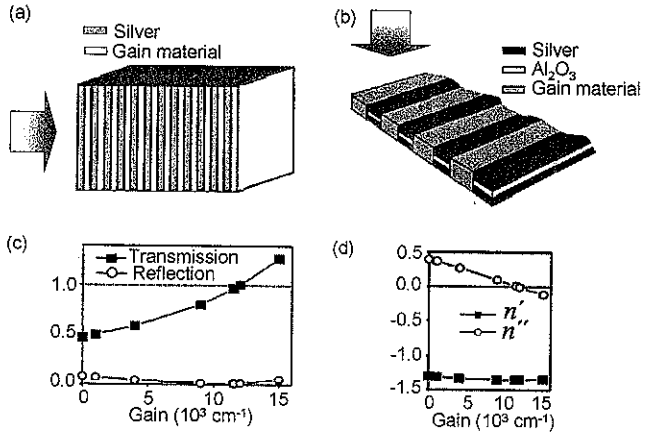

Fig. 5. (a) NIM/PIM stack comprised of metal and gain material layers (Ramakrishna and Pendry [2003]); (b) schematic of a NIM utilizing pairs of metal strips embedded in gain material; (c,d) the transmission and reflection coefficients as well as the real and imaginary parts of the refractive index as functions of gain calculated for the structure shown in (b). (Adapted from Klar, Kildishev, Drachev and Shalaev [2006].)

stack at optical frequencies. In addition, Tretyakov has suggested that both loss and bandwidth limitations can be efficiently reduced in active NIMs (Tretyakov [2001]).

Klar, Kildishev, Drachev and Shalaev [2006] proposed immersing the NIM's meta-atoms such as pairs of metal nanorods or double silver strips into the gain medium, as shown in fig. 5b. Coatings made of solutions of dye molecules, for example Rhodamine 6G, or semiconductor nanocrystals, such as CdSe, have been suggested as potential candidate materials for practical implementation of this approach. Figures 5c and d show the transmission and reflection coefficients as well as the real and imaginary parts of the refractive index as functions of gain calculated for the structure shown in fig. 5b. In this case the structure was illuminated with a plane wave at a wavelength of 584 nm from above. It shows that the structure becomes transparent at a gain level of 12,000 cm^{-1}, while the real part of the refractive index is practically unaffected by the presence of the gain material.

Finally, Popov and Shalaev [2006a, 2006b] proposed an alternative way of compensating losses in optical NIMs by efficient optical parametric amplification enabled by new "backward" phase-matching conditions that will be discussed in § 6.2.

2.3. Alternative approaches to negative refraction

Several alternative approaches to the realization of NIMs have been suggested, including photonic crystals (PC) (Notomi [2000]), anisotropic waveguides (Podolskiy and Narimanov [2005b]), organic and uniaxial gyrotropic crystals and a thin film on a metal substrate (Agranovich, Shen, Baughman and Zakhidov [2004b], Agranovich, Gartstein and Zakhidov [2006]), nanotransmission lines (Engheta, Salandrino and Alu [2005]), frequency-selective surfaces (Alu and Engheta [2005b], Khoo, Williams, Diaz, Chen, Bossard, Werner, Graugnard and Summers [2006]) and three- and four-level atomic systems (Oktel and Müstecaplıoglu [2004], Thommen and Mandel [2006]).

2.3.1. Photonic crystals

In this subsection we discuss NIMs properties that can be achieved in PCs (Kosaka, Kawashima, Tomita, Notomi, Tamamura, Sato and Kawakami [1998], Notomi [2000], Gralak, Enoch and Tayeb [2000], Luo, Johnson, Joannopoulos and Pendry [2002], Foteinopoulou, Economou and Soukoulis [2003], Foteinopoulou and Soukoulis [2003], Parimi, Lu, Vodo and Sridhar [2003], Cubukcu, Aydin, Ozbay, Foteinopoulou and Soukoulis [2003a, 2003b], Berrier, Mulot, Swillo, Qiu, Thylén, Talneau and Anand [2004] and Schonbrun, Tinker, Park and Lee [2005]). PCs are dielectric or metallic structures periodically modulated on the scale of a wavelength that allow electromagnetic radiation of certain wavelengths to enter their structure but block other spectral components in a fashion analogous to the semiconductor bandgap (Yablonovitch [1987], John [1987]). PCs composed of dielectric materials have the important advantage of significantly lower loss compared to metallic NIMs at optical frequencies. While many applications of PCs rely on the presence of the photonic bandgap, interesting spatial and temporal effects, including negative refraction, have been predicted and demonstrated at frequencies outside the bandgap (Russell [1991], Lin, Hietala, Wang and Jones [1996], Eggleton, Slusher, de Sterke, Krug and Sipe [1996], Litchinitser, Eggleton and Patterson [1997], Kosaka, Kawashima, Tomita, Notomi, Tamamura, Sato and Kawakami [1998], Notomi [2000], Ozbay, Bulua, Aydina, Caglayana and Guvena [2004]).

Notomi [2000] has pointed out that in weakly modulated photonic crystals the effective refractive index cannot be defined because the propagation direction depends on angle of incidence and wavelength, and represents a diffraction phenomenon. In strongly modulated photonic crystals, however, light propagation becomes refraction-like in the vicinity of the photonic band gap, where the effective refractive index can be defined. Its sign and the absolute value can

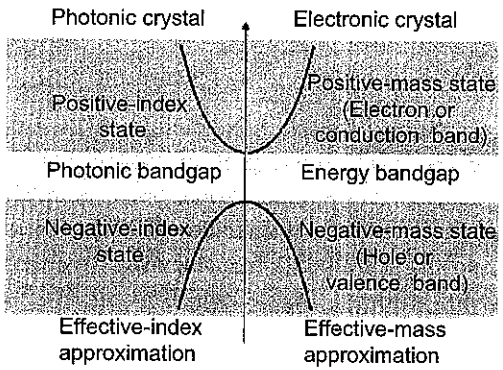

Fig. 6. Analogy between effective-mass approximation for Bloch electron bands and effective-index approximation for Bloch photon bands. (Adapted from Notomi [2000].)

be varied by varying the crystal structure, the refractive indices of composing materials, and the wavelength. The effective index can be negative or less than unity.

Finally, there is an interesting analogy between the photonic bandgap in PCs and the electronic bandgap in semiconductors, as shown in fig. 6. In a semiconductor, a negative-effective-mass state appears below the energy gap, and a positive-effective-mass state is above the gap. A similar behavior is seen for the effective refractive index in PCs. This is not surprising because the sign of the effective mass in semiconductors and the sign of the effective index in photonic crystals are both derived from the band curvature. Also, the effective-mass approximation is only valid near the bandgap. Similarly, the effective-index approximation is only valid near the photonic bandgap.

While a negative refraction can indeed be realized in PCs, and has recently been demonstrated in the near infrared frequency region by Berrier, Mulot, Swillo, Qiu, Thylén, Talneau and Anand [2004], and Schonbrun, Tinker, Park and Lee [2005], not all unusual properties predicted for homogeneous NIMs can be observed straightforwardly in PCs. For instance, the amplification of evanescent field components contributing to super-resolution predicted by Pendry [2000] can only be realized to some extent in PCs. This is due to the fact that for the very large k-vector components responsible for the resolution of the smallest features, the PC cannot be considered as an effective medium and thus there is an upper limit on the transverse wavevector of evanescent components that can be amplified (Luo, Johnson, Joannopoulos and Pendry [2002]).

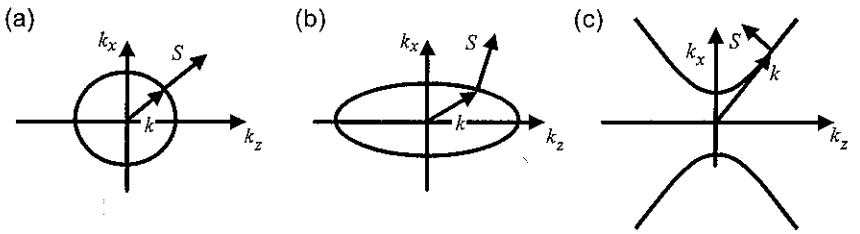

Fig. 7. Isofrequency curves and relative directions of the wavevector k and the Poynting vector S for (a) isotropic material, (b) material with $\varepsilon_x, \varepsilon_z > 0$, (c) material with $\varepsilon_x < 0$, $\varepsilon_z > 0$. (Adapted from Alekseyev and Narimanov [2006].)

2.3.2. *Anisotropic waveguides*

Another non-magnetic, non-resonant approach to the realization of negative refraction with low losses utilizes uniaxial dielectrics with negative dielectric permittivity along the anisotropy axis (Belov [2003], Podolskiy and Narimanov [2005a], Podolskiy, Alekseyev and Narimanov [2005], Alekseyev and Narimanov [2006]). Figure 7 shows isofrequency curves and relative directions of the vectors S and k for a lossless isotropic medium and for the two cases of uniaxial anisotropy ($\varepsilon_x, \varepsilon_z > 0$ and $\varepsilon_x < 0$, $\varepsilon_z > 0$). In the anisotropic case the optical axis is pointing along the x axis. Since ordinary waves are not affected by the anisotropy, only extraordinary polarization is considered. In the isotropic case, the wavevector surfaces are circles, and therefore $S \propto \nabla_k \omega(k) \propto k$, i.e. the vectors S and k are collinear (fig. 7a). For $\varepsilon_x \neq \varepsilon_z$, $\varepsilon_x, \varepsilon_z > 0$, the wavevector surfaces become ellipsoidal and, as a result, the angle between S and k is non-zero (fig. 7b). Finally, for a material with negative transverse dielectric permittivity $\varepsilon_x < 0$ and positive in-plane permittivity $\varepsilon_z > 0$, the dispersion relation becomes hyperbolic. The curvature of the hyperbola is such that S_z and k_z have opposite signs (fig. 7c).

The z-component of the Poynting vector for the extraordinary wave can be written as

$$S_z = \frac{k_z}{2\omega\varepsilon_x} H^2. \tag{2.3}$$

Therefore, if $\varepsilon_x < 0$, S_z is also negative, and thus S_z is opposite to the direction of the wavevector component k_z. This opposite directionality leads to a (effective) negative refractive index for refraction at an interface and for light propagation in a waveguide. In particular, an effective negative refractive index has been predicted for a waveguiding system when anisotropic material with $\varepsilon_x < 0$ and $\varepsilon_z > 0$ is used as the core of a planar (in the y–z plane) waveguide with metal walls. In this case modes with negative group velocity arise (Podolskiy and

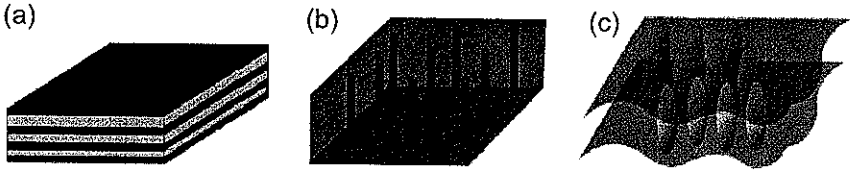

Fig. 8. Metamaterial structures for the potential realization of an anisotropic dielectric response at IR and optical frequencies: (a) layered structure based on semiconductor quantum wells or layered plasmonic or polar materials; (b) aligned plasmonic nanowires with negative ε_{pl} embedded in a dielectric host with positive ε_h; (c) composite of spheroidal inclusions in an isotropic host.

Narimanov [2005a]); for these modes the wavevector and the energy flux are antiparallel.

Although this approach has not yet been realized experimentally, several metamaterial-based structures have been proposed for the realization of the required anisotropic dielectric response at the IR and optical frequencies, as shown in fig. 8. These include:

(a) A layered structure based on multiple semiconductor quantum wells (Podolskiy and Narimanov [2005b]) or on layered plasmonic (Au, Ag, Al) or polar (SiC) materials (Shvets [2003]) (fig. 8a).

(b) A two-dimensional structure based on an array of aligned plasmonic nanowires with $\varepsilon_{pl} < 0$ embedded in a dielectric host with $\varepsilon_h > 0$ (Wangberg, Elser, Narimanov and Podolskiy [2006]) (fig. 8b).

(c) A composite structure of sub-wavelength anisotropic (e.g. spheroidal) inclusions in an isotropic dielectric host (fig. 8c).

2.3.3. *Other designs*

In addition, several other promising possibilities of realization of NIMs at optical frequencies have been suggested.

Agranovich, Shen, Baughman and Zakhidov [2004a] suggested the possibility of realizing negative refraction at optical frequencies in a number of non-magnetic media including bulk waves in organic crystals and in gyrotropic materials.

In organic crystals, the effective mass of the Frenkel exciton can be designed to be negative, leading to a negative spatial dispersion for the exciton. This dispersion in turn leads to the appearance of additional exciton–polariton waves with a negative group velocity (shown in fig. 9a).

Negative exciton–polariton dispersion also occurs in cubic or uniaxial gyrotropic crystals. The dispersion curve of excitons splits into two branches that couple with the light of two different circular polarizations to form two exciton–

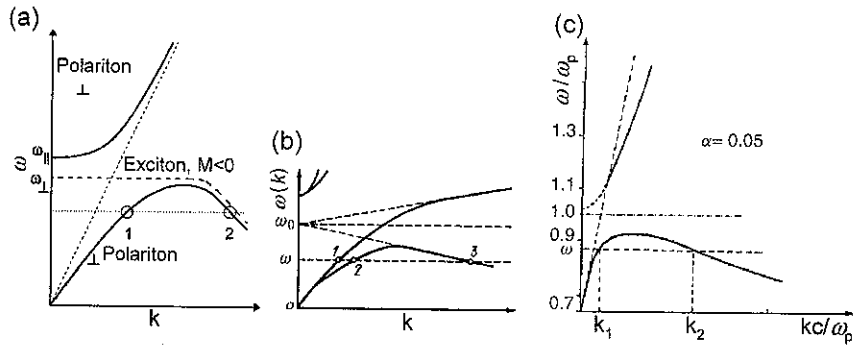

Fig. 9. (a) Dispersion curve of exciton–polaritons near an exciton resonance. The polariton waves near point 2 have a negative group velocity. (b) Dispersion of polaritons in a cubic gyrotropic crystal near exciton resonance (or in uniaxial crystals with the wavevector along the optical axis); curves 1 and 2 correspond to right and left circular polarizations, polaritons in region 3 have a negative group velocity. (c) Surface plasmon dispersion of metal covered by a thin metal film for a particular set of parameters. (Adapted from Agranovich, Shen, Baughman and Zakhidov [2004b].)

polariton branches, one of which (lower branch) has a section with a negative slope corresponding to a negative group velocity as shown in fig. 9b.

Opposite directionality of the group and phase velocities can also be realized in a structure consisting of a thin film on a metal substrate. When surface polaritons propagate along a metal surface covered with a thin film with a dipole resonance, gaps open up in the surface plasmon–polariton spectrum. As in the previous two cases, the lower branch of the surface polariton dispersion curve has a negative slope as shown in fig. 9c, and the corresponding surface polaritons exhibit a negative group velocity. However, it should be mentioned that losses associated with this structure may be significant.

Engheta, Salandrino and Alu [2005] have shown theoretically that plasmonic and non-plasmonic nanoparticles that are significantly smaller than a light wavelength behave as nanoinductors and nanocapacitors, respectively, as shown in fig. 10a. When fused together, nanoparticles with positive and negative permittivities form parallel and serial nanoelements that can be arranged into optical nanotransmission lines. Two examples of such nanotransmission lines are shown in fig. 10b: series nanoinductors and shunt nanocapacitors providing a conventional transmission line operating in the optical regime (left), and shunt nanoinductors and series nanocapacitors forming a negative-index optical transmission line (right).

Khoo, Williams, Diaz, Chen, Bossard, Werner, Graugnard and Summers [2006] have designed a metallo-dielectric frequency selective surface (FSS) that exhib-

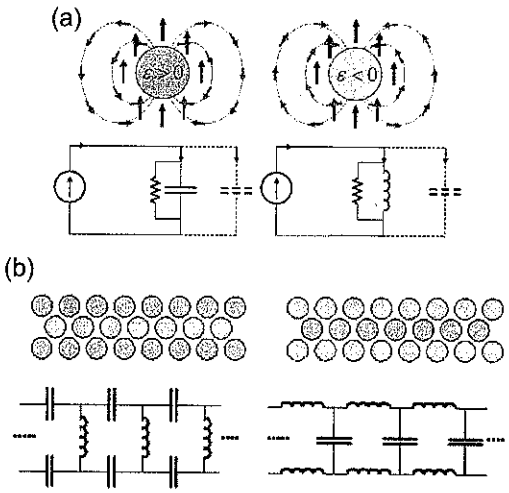

Fig. 10. (a) Nanoparticles behaving as nanocapacitors and nanoinductors. (b) Left: a conventional transmission line operating in the optical regime; right: a negative-index transmission line. (See Engheta, Salandrino and Alu [2005].)

ited a refractive index with a negative real part ranging from -1.6 to -1.0 and a very small imaginary part, i.e. very low loss in the wavelength range around 3 μm. The FSS structure consisted of a 120 nm-thick silver screen sandwiched between two 0.508 μm-thick polyimide films with the unit cell size of the FSS of 2.75×2.75 μm^2. Also, it has been suggested that by incorporating a liquid crystal as an overlay onto these FSS-based structures it is feasible to design NIMs tunable in a wide range of frequencies in the visible and infrared ranges.

Finally, the possibility of realization of electromagnetically induced negative refractive properties in three-level and four-level atomic media was proposed by Oktel and Müstecaplıoglu [2004] and Thommen and Mandel [2006], respectively. These systems would have the advantage of being homogeneous and not requiring any periodicity.

§ 3. Negative refraction and superlens

3.1. *Negative refraction*

Negative refraction is one of the basic consequences of negative n. For a plane wave propagating from one medium into another the boundary conditions are

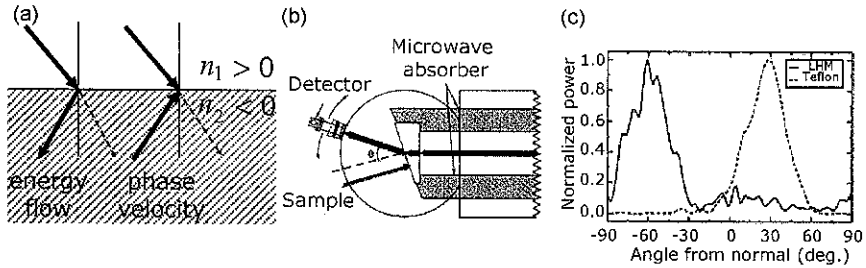

Fig. 11. (a) Negative refraction at NIM interface. (b) Experimental setup used for the demonstration of negative refraction. (c) Experimental results: transmitted power as a function of the refraction angle for a Teflon sample (dashed curve) and for a NIM sample (solid curve). (Adapted from Shelby, Smith and Shultz [2001].)

given by

$$E_t^{(1)} = E_t^{(2)}, \qquad H_t^{(1)} = H_t^{(2)},$$
$$\varepsilon_1 E_z^{(1)} = \varepsilon_2 E_z^{(2)}, \qquad \mu_1 H_z^{(1)} = \mu_2 H_z^{(2)}. \tag{3.1}$$

These equations indicate that while the transverse components of the fields (denoted by a subscript "t") are not affected by the signs of ε and μ, the longitudinal components (denoted by a subscript "z") are. Negative refraction and the opposite directionality of the vectors k and S are illustrated in fig. 11a. While the Poynting vector is always directed away from the interface between the two media, the propagation vector k points towards the interface in NIMs.

Figure 11b shows the experimental setup used in the first experiment demonstrating negative refraction (Shelby, Smith and Schultz [2001]). In this experiment, the deflection of a beam of microwave radiation was measured as the beam passed through a prism-shaped sample of NIM or a conventional PIM material (Teflon) for comparison. Figure 11c shows the transmitted power as a function of the refraction angle for both the Teflon sample (dashed curve) and the NIM sample (solid curve). Later, negative refraction was also reported by Houck, Brock and Chuang [2003].

Another interesting consequence of the refractive index being negative is the possibility of constructing an imaging system based on a flat slab of NIM with $n = -1$ surrounded by a conventional medium with $n = 1$, which was first discovered by Veselago [1968].

A truly remarkable finding was made by Pendry [2000], who noticed that a flat slab of NIM under appropriate conditions would not only focus propagating (or far-field) components emanating from the source, but also recover the evanescent

(near-field) components that cannot be refocused by a conventional lens. Thus, Pendry named it a "superlens".

3.2. Superlens

The resolution of a conventional optical imaging system is limited by the wavelength of incoming light. The reason for the limited resolution is diffraction and the incapability of conventional imaging devices to re-focus evanescent field components. Consider an object and a lens placed along the z-axis so that the light from the object is propagating in the positive z direction. The field radiated from the object can be written in terms of its angular spectrum as

$$E(x, y, z, t) = \sum A(k_x, k_y) \exp\left[\mathrm{i}(k_z z + k_y y + k_x x - \omega t)\right], \tag{3.2}$$

where

$$k_z = \sqrt{\omega^2/c^2 - \left(k_x^2 + k_y^2\right)}$$

and only the positive square root is taken since the energy is propagating in the positive z direction. As long as $(k_x^2 + k_y^2) < \omega^2/c^2$, all k_z components are real and propagating and, therefore, phase correction is required to re-focus them in the image plane. However, if $(k_x^2 + k_y^2) > \omega^2/c^2$, k_z becomes imaginary, and the wave becomes an evanescent wave decaying along the positive z direction before reaching the image plane. The challenge here is that such waves decay in amplitude and, therefore, in order to focus them, amplitude correction (i.e. amplification) is required. Conventional lenses can only perform phase correction. Thus, evanescent components, responsible for the high-frequency and correspondingly small-scale features of the object, are usually lost in conventional imaging systems as illustrated in fig. 12a. The highest resolution can be estimated in terms of optical wavelength as follows:

$$k_{\max} \approx \frac{\omega}{c} = \frac{2\pi}{\lambda}, \quad \text{and therefore,} \quad \Delta x_{\min} \approx \lambda. \tag{3.3}$$

More precisely, the diffraction limit or Abbe limit for a conventional lens is given by $\Delta x = \lambda/(2n \sin\alpha)$, where λ, n and α are the wavelength of light, the refractive index of the medium in object space (immersion material), and the semi-aperture angle of the lens, respectively. Therefore, Δx can be estimated as $\Delta x_{\min} \approx \lambda/(2n)$, which is limited by the wavelength and the refractive index of available transparent immersion media.

As mentioned above, Veselago [1968] noted that a planar slab of material with a refractive index of $n = -1$ and $\varepsilon = \mu = -1$ in air ($n = \varepsilon = \mu = 1$) can

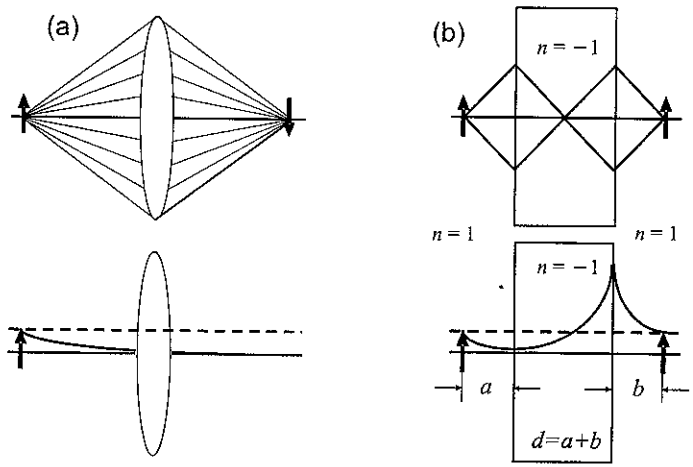

Fig. 12. (a) Propagating (upper plot) and evanescent (lower plot) field components processed by a conventional lens; (b) propagating (upper plot) and evanescent (lower plot) field components processed by "Pendry's" superlens.

produce an image of a point source as shown in the upper plot in fig. 12b. In a negative-index slab, diverging rays from an object are negatively refracted at the first surface of the slab, reversing their trajectories so that they form an image first within the slab, and then a second one outside the slab. Moreover, no reflection at the interfaces occurs owing to impedance matching. It is noteworthy that Veselago's "planar lens" differs from a conventional lens in several respects: (1) it does not require any curvature, (2) it cannot focus parallel rays, (3) it does not have an optical axis, and (4) it cannot provide any magnification, i.e. its magnification is always unity.

One of the most unusual properties of a planar slab of NIM was first realized by Pendry [2000], who found that a slab with refractive index $n = -1$ surrounded by air ($n = 1$) not only focuses the propagating field components but can also restore the evanescent field components, potentially improving the resolution in the image plane as schematically shown in the lower plot in fig. 12b. Thus, such a NIM slab has been called a "superlens". The unique properties of such superlenses have stimulated an enormous interest as well as debates among researchers (Pendry [2000], 't Hooft [2001], Williams [2001], Garcia and Nieto-Vesperinas [2002], Shen and Platzman [2002], Ye [2003], Lagarkov and Kissel [2004], Merlin [2004], Larkin and Stockman [2005], Podolskiy and Narimanov [2005a], Jacob, Alekseyev and Narimanov [2006], Taubner, Korobkin, Urzhumov, Shvets and Hillenbrand [2006], Blaikie, Melville and Alkalsi [2006]).

Owing to the opposite directionality of the phase velocity and the energy velocity in NIMs, for the waves propagating in the positive z direction

$$k_z' = -\sqrt{\omega^2/c^2 - (k_x^2 + k_y^2)}.$$

For the evanescent components the transmission coefficient is given by $T = \exp(\alpha d)$, where

$$\alpha = \sqrt{(k_x^2 + k_y^2) - \omega^2/c^2}.$$

Therefore, the evanescent waves emerge from the far side of the slab enhanced in amplitude. This does not violate energy conservation because evanescent waves carry no energy.

Figure 12b (lower plot) shows schematically an evanescent wave exponentially decaying away from an object and growing exponentially within the planar negative index slab. In the right half-space outside of the slab, the wave decays again until it reaches the image plane. Thus, the resolution limit of the planar negative index slab is determined by the number of evanescent field components from the object that can be recovered, rather than by the diffraction limit.

However, in order to refocus those evanescent field components, the thickness d of the slab, the distance a between the object and the slab surface, and the distance b between the image and the slab surface must all be small in comparison to the wavelength. Otherwise, the evanescent wave components from the object decay to a level that their retrieval becomes unattainable due in particular to material losses of the slab. It has been shown that even a very small loss would cancel a superlensing effect (Podolskiy and Narimanov [2005a], Podolskiy, Kuhta and Milton [2005]). Recently, several ideas for converting the evanescent field components into propagating components, potentially increasing the resolution in the far-field zone, have been discussed by Durant, Liu, Fang and Shang [2006], Salandrino and Engheta [2006], and Jacob, Alekseyev and Narimanov [2006]. In addition, Smolyaninov, Hung and Davis [2006] have proposed and experimentally demonstrated a new design for a magnifying superlens in the visible range.

An important limit is when the dimensions (a, d, b) of a system are much smaller than the wavelength, the electric and magnetic fields decouple, and the requirement for superlensing of the TM wave is reduced to only $\varepsilon_{\text{slab}} = -\varepsilon_{\text{h}}$, where ε_{h} is the permittivity of the host material surrounding the lens (Pendry [2000]). The corresponding condition for TE-wave superlensing is only $\mu_{\text{slab}} = -\mu_{\text{h}}$, where μ_{h} is the permeability of the host material surrounding the lens. The condition $\varepsilon_{\text{slab}} = -\varepsilon_{\text{h}}$ corresponds to the condition for excitation of the surface plasmon resonance in a metal slab. This plasmon resonance is responsible for the building up of electromagnetic energy, which enables the exponential growth of evanescent components. A slab of silver illuminated at its surface plasmon resonance has already been used to demonstrate growth of evanescent waves, submicron imaging, and imaging well beyond the diffraction limit (Liu, Fang, Yen and Zhang [2003], Melville, Blaikie and Wolf [2004], Melville and Blaikie [2005], Fang, Lee, Sun and Zhang [2005]). Although limited to the near-field zone, this kind of near-field superlens is likely to find many applications, including biomedical imaging and nanolithography. One of the limitations associated with a lens based on a bulk metal is that its operation is limited to a single wavelength satisfying the condition $\varepsilon_{\text{slab}}(\lambda) = -\varepsilon_{\text{h}}$. To overcome this limitation a superlens based on metal–dielectric composites has been proposed (Cai, Genov and Shalaev [2005]). The operation wavelength of such lens can be controlled by the metal filling factor of the composite.

Pokrovsky and Efros [2003] have proposed another lens configuration, based on a flat slab of NIM. In contrast to the "Veselago" lens described above, the only condition that the new lens must satisfy is $n_2 = -n_1$, but $\varepsilon_2 \neq -\varepsilon_1$ and $\mu_2 \neq -\mu_1$. The most important difference between the new type of lens and the "Veselago" lens is the presence of reflected waves. As a consequence, the new lens produces a periodic array of 3D images of different intensities. Since only one condition has to be satisfied instead of the two ($\varepsilon_2 = -\varepsilon_1$ and $\mu_2 = -\mu_1$) in Veselago's design, this new lens should be easier to fabricate.

§ 4. Enhanced nonlinearity and its origin in metamaterials

As discussed in the introduction, the interactions of the magnetic field component with conventional materials may become significant only at very high intensities of $\sim 10^{18}$ W/cm^2. On the other hand, metamaterials that enable the magnetic field component even in a linear regime are expected to give rise to a plethora of new nonlinear phenomena at moderate intensities used in conventional nonlinear optics.

The majority of studies of NIMs to date have focused on linear properties, assuming that the dielectric permittivity ε and magnetic permeability μ are *independent of the intensity* of the electromagnetic field. The nonlinear properties of NIMs, where one or both material parameters are *intensity-dependent*, are not fully explored. However, even initial studies have already predicted novel fundamental properties of NIMs and entirely new regimes of nonlinear interactions. In this section we discuss the effects of NIM micro- or nanostructure on their nonlinear response.

Zharov, Shadrivov and Kivshar [2003] have investigated the nonlinear response of a two-dimensional NIM periodic structure consisting of arrays of metallic wires

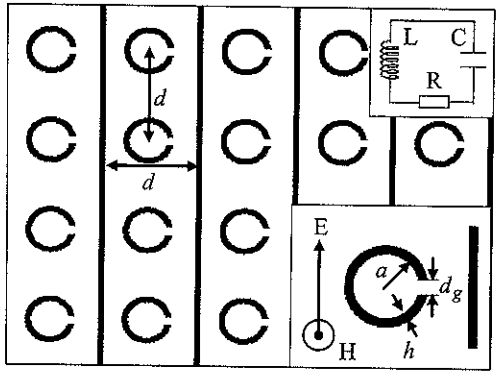

Fig. 13. Schematic of composite metamaterial structure. The lower inset shows a unit cell of the periodic structure. The upper inset shows the SRR equivalent oscillator. (See Zharov, Shadrivov and Kivshar [2003].)

and SRRs embedded into a nonlinear dielectric and operating at microwave frequencies (fig. 13). The metallic wires are responsible for the negative sign of the effective dielectric permittivity, and the SRRs provide the negative sign of the magnetic permeability.

Two important contributions to the nonlinear properties of this structure have been identified. The first originates from the intensity-dependent part of the effective dielectric permittivity of the nonlinear dielectric host material, $\varepsilon_D = \varepsilon_D(|E|^2)$. Then, for the electric field orientation along the wires as shown in fig. 13, the effective nonlinear dielectric permittivity is obtained in the form

$$\varepsilon_{\text{eff}} = \varepsilon_D\big(|E|^2\big) - \frac{\omega_p^2}{\omega(\omega - i\gamma_e)}, \tag{4.1}$$

where $\omega_p \approx (c/d)[2\pi/\ln(d/r)]^{1/2}$ is the effective plasma frequency, c is the speed of light, d is the lattice constant, r is the wire radius, and $\gamma_e = c^2/2\sigma S\ln(d/r)$, with σ the conductivity of the wire metal, and S the effective area of the wire cross-section.

The second contribution originates from the periodic structures of resonators, since the SRR capacitance depends on the strength of the local electric field in a narrow slot. The effective magnetic permeability has been found in the form

$$\mu_{\text{eff}} = 1 + \frac{F\omega^2}{\omega_{0\text{NL}}^2(H) - \omega^2 + i\Gamma\omega}, \tag{4.2}$$

where $\omega_{0\text{NL}}^2(H) = (c/a)^2 d_g/\pi h\varepsilon_D(|E_g(H)|^2)$ is the eigenfrequency of oscillations in the presence of the external field, h is the width of the ring, $F = \pi a^2/d^2 \ll 1$, $\Gamma = c^2/(2\pi\sigma a h)$ if h is smaller than the thickness of the skin layer δ, and $\Gamma = c^2/(2\pi\sigma a\delta)$ for $h > \delta$. Equation (4.2) shows that the resonant frequency of the array of the SRRs depends on the amplitude of the external magnetic field and, consecutively, leads to the intensity-dependent μ_{eff}.

The magnetic nonlinearity in this case has been found to be much stronger than the nonlinearity in the dielectric properties owing to the field enhancement in the SRRs. The intensity-dependent μ_{eff} can be switched from positive to negative values, which in turn changes the material properties from PIM to NIM and back. It has been suggested that nonlinear NIMs can be created by inserting nonlinear elements into the slots of SRRs (Zharov, Shadrivov and Kivshar [2003], Lapine, Gorkunov and Ringhofer [2003]). For example, in the microwave range a nonlinear response has been obtained by inserting diodes into the SRRs (Lapine, Gorkunov and Ringhofer [2003]). This approach allows easy tuning of the NIM properties by an external field.

A similar analysis for an SRR array alone and with parameters appropriate for optical frequencies has been performed by O'Brien, McPeake, Ramakrishna and Pendry [2004]; they demonstrated large local fields potentially leading to enhanced nonlinear effects and a bistable switching of the resonance frequency as a function of field strength.

In another study a simple theory supporting experimentally observed SHG in magnetic metamaterials has been proposed (Klein, Enkrich, Wegener and Linden [2006]). Experimental results reported in this work indicate that much larger SHG signals are detected when magnetic-dipole resonances are excited, as compared with purely electric-dipole resonances. These results have been shown to be in a qualitative agreement with calculations based on the magnetic component of the Lorentz force exerted on metal electrons.

§ 5. Optical bistability and solitons

Solitons are fascinating nonlinear phenomena ubiquitous in sciences, including mathematics, optics, quantum mechanics, particle physics and molecular biology. In optics, the term "soliton" refers to a localized pulse that travels without changing its shape, and the difference between a "soliton" and a "solitary wave" is often disregarded. A variety of solitons, including temporal, spatial, spatiotemporal, incoherent, gap and discrete solitons, have been predicted and demonstrated in conventional PIM materials. The existence of solitons relies on the balance of nonlinear and dispersive (or diffractive) effects. Owing to the unique relationship between the phase and energy velocities, strong frequency dependence of

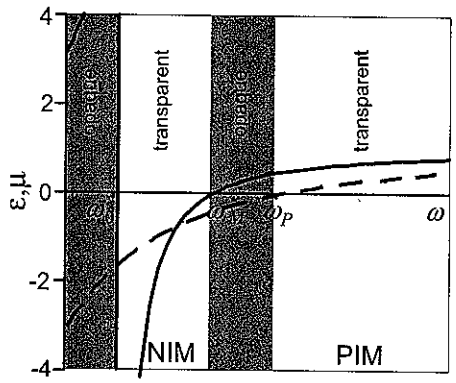

Fig. 14. Frequency-dependent effective dielectric permittivity (dashed line) and effective magnetic permeability (solid line) of the metamaterial. (Adapted from Shadrivov, Zharov and Kivshar [2006].)

the material parameters, and enhanced nonlinearities, new soliton phenomena are anticipated in NIMs.

Recently several aspects of temporal and spatial dynamics and soliton propagation in NIMs have been addressed by Scalora, Syrchin, Akozbek, Poliakov, D'Aguanno, Mattiucci, Bloemer and Zheltikov [2005], Scalora, D'Aguanno, Mattiucci, Akozbek, Bloemer, Centini, Sibilia and Bertolotti [2005], Lazarides and Tsironis [2005], Kourakis and Shukla [2005], Shadrivov, Zharova, Zharov and Kivshar [2005], Shadrivov and Kivshar [2005], Gabitov, Indik, Litchinitser, Maimistov, Shalaev and Soneson [2006], Marklund, Shukla and Stenflo [2006], Kockaert, Tassin, Van der Sande, Veretennicoff and Tlidi [2006], and Tassin, Van der Sande, Veretenov, Kockaert, Veretennicoff and Tlidi [2006].

5.1. *Generalized nonlinear Schrödinger equation*

Figure 14 shows an example of frequency-dependent $\varepsilon(\omega)$ and $\mu(\omega)$. In this example, a negative index of refraction occurs in the frequency range $\omega_0 < \omega < \omega_m$, where ω_0 is the resonant frequency of the metamaterial and both ε and μ are negative. In the frequency range $\omega > \omega_p$, where ω_p is the plasma frequency, the metamaterial possesses PIM properties. In the absence of losses, both NIM and PIM spectral regions are transparent. In the frequency regions $\omega < \omega_0$ and $\omega_m < \omega < \omega_p$, where dielectric permittivity and magnetic permeability have different signs, the refractive index is imaginary and as a result the material is opaque.

Owing to this strong frequency dependence, the optical pulse width is expected to have an important effect on the dynamics of nonlinear pulse propagation in NIMs. The pulse spectrum may overlap with one or more spectral regions in the metamaterial depending on its temporal width and shape (Agranovich, Shen, Baughman and Zakhidov [2004a]). There are two potentially important limits for pulse interactions with NIMs: (1) the wide spectrum of an ultrashort pulse covers frequency regions corresponding to the positive and negative refractive index as well as those where one of the material parameters is negative while the other is positive, and (2) the spectral content of the pulse is very narrow, so that the entire pulse spectrum falls in either the positive- or the negative-index region.

We note here that the strong frequency dependence of the dielectric permittivity and magnetic permeability is one of the most fundamental properties of NIMs; it can be understood as follows: the energy flux density (Poynting vector) in a variable electromagnetic field is defined by eq. (1.2) regardless of whether dispersion is present. Using Maxwell's equations, the rate of change of the energy in a unit volume can be written as

$$-\nabla \cdot S = \frac{1}{4\pi}\left(E\frac{\partial D}{\partial t} + H\frac{\partial B}{\partial t}\right). \tag{5.1}$$

In a dielectric medium without dispersion, when ε and μ are real constants, eq. (5.1) can be regarded as the rate of change of the electromagnetic energy

$$W = \varepsilon E^2 + \mu H^2, \tag{5.2}$$

which would be negative given that both ε and μ are less than zero. However, in a transparent dispersive medium the mean value of the electromagnetic energy is defined as

$$\overline{W} = \frac{\partial(\omega\varepsilon)}{\partial\omega}\overline{E^2} + \frac{\partial(\omega\mu)}{\partial\omega}\overline{H^2}. \tag{5.3}$$

Equation (5.3) shows that in order for the total energy to be positive when both ε and μ are negative, it is necessary that

$$\frac{\partial(\omega\varepsilon)}{\partial\omega} > 0, \qquad \frac{\partial(\omega\mu)}{\partial\omega} > 0, \tag{5.4}$$

which implies that $\varepsilon(\omega)$ and $\mu(\omega)$ must be frequency dependent.

Scalora, Syrchin, Akozbek, Poliakov, D'Aguanno, Mattiucci, Bloemer and Zheltikov [2005, see also the Erratum] derived a generalized nonlinear Schrödinger equation taking into account the frequency dependence of both dielectric permittivity and magnetic permeability and describing the propagation of ultrashort pulses in NIMs and, in fact, in a more general class of magnetically active

metamaterials:

$$\frac{\partial E}{\partial z} \approx \frac{ik''}{2}\frac{\partial^2 E}{\partial t^2} + \frac{i\beta\mu\chi^{(3)}}{2n}\left[1 - \frac{\mu\chi^{(3)}}{4n^2}|E|^2\right]|E|^2 E + \chi^{(3)}\left\{\frac{\mu}{2V_g n^2} - \frac{\gamma+\mu}{2n}\right\}\frac{\partial t(|E|^2 E)}{\partial t}, \tag{5.5}$$

where E is the electric field envelope function (not necessarily slowly varying), $\chi^{(3)}$ is the cubic nonlinearity coefficient, k'' is the group velocity dispersion coefficient given by

$$k'' = \frac{\partial}{\partial\omega}\left(\frac{1}{V_g}\right) = \frac{1}{\beta n}\left(\frac{1}{V_g^2} - \alpha\gamma - \beta\frac{\varepsilon\gamma' + \mu\alpha'}{4\pi}\right), \tag{5.6}$$

and the coefficients α, α', γ, and γ' are defined as

$$\alpha = \frac{\partial[\tilde{\omega}\varepsilon(\tilde{\omega})]}{\partial\tilde{\omega}}, \qquad \alpha' = \frac{\partial^2[\tilde{\omega}\varepsilon(\tilde{\omega})]}{\partial\tilde{\omega}^2},$$
$$\gamma = \frac{\partial[\tilde{\omega}\mu(\tilde{\omega})]}{\partial\tilde{\omega}}, \qquad \gamma' = \frac{\partial^2[\tilde{\omega}\mu(\tilde{\omega})]}{\partial\tilde{\omega}^2},$$

V_g is the group velocity, $\beta = 2\pi\tilde{\omega}$, $\tilde{\omega} = \omega/\omega_p$, ω_p is the plasma frequency.

Equation (5.5) uncovers several new features that are distinct from a standard NLSE derived for non-magnetic materials. The linear and nonlinear coefficients can be tailored through the linear properties of the medium to attain any combination of signs unachievable in conventional materials, thus having a significant potential for the realization of a wide class of solitary waves. In particular, the sign of the group-velocity dispersion can be positive or negative and is determined by the particular choice of ε and μ parameters [eq. (5.6)]. Also, assuming a positive $\chi^{(3)}$, the sign of the leading nonlinear coefficient is always positive because the ratio μ/n is positive. Therefore, both bright and dark soliton solutions have been predicted to emerge depending on the sign of the group velocity. On the other hand, the pseudo-$\chi^{(5)}$ correction term is proportional to $(-\mu^2/n^3)$, which makes the coefficient positive. Therefore, its effect is to enhance the nonlinearity, which is in sharp contrast to the case of conventional materials where the effect of this term is to quench the nonlinearity.

5.2. *Solitons in plasmonic nanostructures*

Gabitov, Indik, Litchinitser, Maimistov, Shalaev and Soneson [2006] have considered short-pulse propagation in the simplest case of a nanostructure consisting

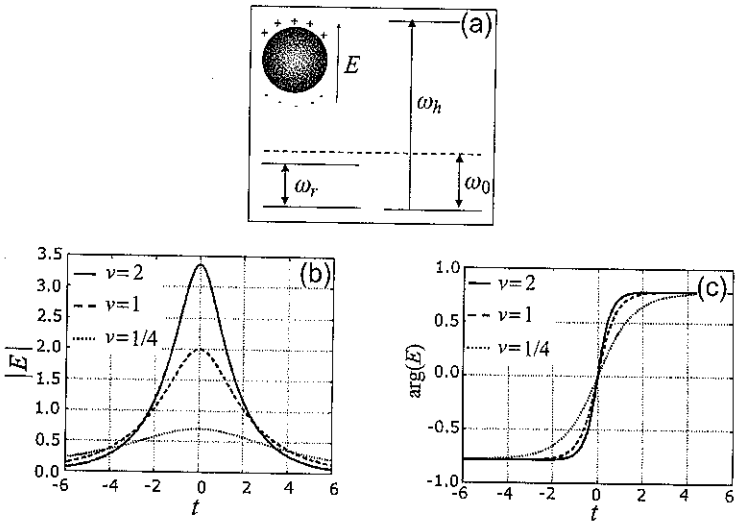

Fig. 15. (a) Schematic of transitions in a nanostructure consisting of metallic nanoparticles embedded in a glass host (ω_r is the frequency of plasmonic oscillations, ω_0 is the light carrier frequency, ω_h is the resonance frequency of the host material); (b,c) soliton amplitude and phase for three different soliton velocities.

of metallic nanoparticles embedded in a glass host, such that the resonance frequencies of the host medium are well separated from those of the nanoparticles, as schematically shown in fig. 15a. Examples include silver or gold spherical or spheroidal nanoparticles embedded in SiO_2. In these cases, the plasmonic resonance frequencies are in the visible part of the spectrum, whereas the resonance of the host is in the ultraviolet. Although this structure possesses only an electric resonance (i.e. resonance of ε) and, therefore, does not produce a negative refractive index, it has been found that it provides a good simplified model providing important insight into the nonlinear optical properties of more complex structures such as plasmonic NIMs.

The origin and magnitude of third-order nonlinearity in such nanostructures are well characterized theoretically and experimentally (Uchida, Kaneko, Omi, Hata, Tanji, Asahara, Ikushima, Tokizaki and Nakamura [1994], Rautian [1997], Drachev, Buin, Nakotte and Shalaev [2004]). In particular, it has been shown that quantum effects in metal nanoparticles driven by a resonant optical field play an important role in inducing a strong nonlinear response (Drachev, Buin, Nakotte and Shalaev [2004]).

Light interaction with metal nanoparticles can be described by a system of equations consisting of Maxwell's equation for the electric field and an oscil-

lator equation describing the displacement of conduction electrons in the metal nanoparticles from equilibrium (plasmonic oscillations). Assuming pulse dynamics to vary on a scale that is much slower than the plasmonic, host atom, and carrier wave oscillations, the interaction of the electric field with plasmonic oscillations in nanoparticles in the presence of this cubic nonlinearity can be described by the forced Duffing equation in the slowly varying envelope approximation,

$$\mathrm{i}\frac{\partial Q}{\partial t} + (\omega_\mathrm{r} - \omega_0)Q + \frac{3\gamma}{2\omega_0}|Q|^2 Q = -\frac{e}{2m\omega_0}E, \tag{5.7}$$

where E and Q are the slowly varying envelopes of the electric field and plasmonic oscillations, respectively, t is time, γ is the coefficient of nonlinearity, and e and m are the electron charge and rest mass. The equation for the electric field envelope is

$$\mathrm{i}\left(\frac{\partial E}{\partial z} + \frac{1}{v_\mathrm{g}}\frac{\partial E}{\partial t}\right) = -\frac{2\pi\omega_0 N_\mathrm{p} e}{cn_0}\langle Q\rangle - \frac{2\pi\omega_0 N_\mathrm{a}|d|^2}{cn_0\hbar\Delta_\mathrm{a}}E - \frac{2\pi\mathrm{i}\omega_0 N_\mathrm{a}|d|^2}{cn_0\hbar\Delta_\mathrm{a}^2}\frac{\partial E}{\partial t}, \tag{5.8}$$

where z is the propagation coordinate, v_g is the group velocity, c is the speed of light, n_0 is the refractive index evaluated at the carrier frequency ω_0, and N_p is the product of conduction electron density N and the metal-filling factor p. The parameter N_a is the concentration of host atoms, d is the projection of the dipole matrix element in the direction of the electric field polarization, and $\Delta_\mathrm{a} = \omega_\mathrm{h} - \omega_0$ is the detuning from the resonance frequency of the host atoms. The last two terms in eq. (5.8) are the additional corrections to the refractive index and group index accounting for the off-resonance interaction with the host medium (taken as an ensemble of two-level atoms). Equations (5.7)–(5.8) represent a generalization of the classical Maxwell–Lorentz model and are referred to as the Maxwell–Duffing model. Solitary-wave solutions of eqs. (5.7)–(5.8) have been found analytically by Gabitov, Indik, Litchinitser, Maimistov, Shalaev and Soneson [2006]. These are four-parameter solutions characterized by solitary wave velocity, frequency, phase shift, and the initial pulse position. Electric field amplitudes and phases of the solitary waves are shown in figs. 15b and c for different soliton velocities. Numerical simulations of the Maxwell–Duffing system of equations have indicated that input Gaussian pulses with sufficient amplitudes evolve to stable solitary waves and exhibit behavior analogous to the self-induced transparency in the Maxwell–Bloch system. The simulations have also revealed that the collision dynamics is strongly dependent on initial solitary wave parameters, leading to principally different regimes of interactions: in one regime the collisions are

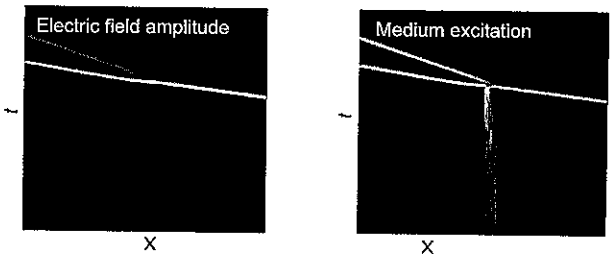

Fig. 16. Electric field and medium excitation corresponding to an inelastic collision resulting in the formation of a "hot spot" – a region where the energy of the solitary wave is transferred to the material excitation.

quasi-elastic, in another regime the collisions are inelastic and at certain parameters result in the development of "hot spots" – regions where the energy of the solitary wave is transferred to the material excitation shown in fig. 16. The formation of such hot spots represents a form of light trapping and, therefore, has high potential for developing phase-controlled optical storage applications.

As already mentioned, understanding the properties of light propagation in a nanostructure consisting of metallic nanoparticles embedded in a glass host is useful for studying wave dynamics in NIMs that simultaneously possess electric and magnetic resonances. A particular case of a nanostructure with a nonlinear electric response and a linear magnetic response was analyzed by Gabitov, Indik, Litchinitser, Maimistov, Shalaev and Soneson [2006]. It was found that the governing nonlinear equations for the electric and magnetic fields decouple, resulting in a system of equations very similar to that derived for the simplest nanostructures composed of metallic nanoparticles when $\mu = 1$. Therefore, many of the results obtained for the simple structure are relevant for NIMs with a nonlinear electric response and a linear magnetic response.

Although only the effects of nonlinear polarization have been analyzed, the contribution of magnetic nonlinearities may be even more pronounced than that of electric nonlinearities (Zharov, Shadrivov and Kivshar [2003]). Therefore, a potentially important extension of this work would take into account nonlinear polarization and nonlinear magnetization as well as the effects of a particular nanostructure.

5.3. Gap solitons

Conventional one-dimensional layered periodic structures composed of two PIMs possess a photonic bandgap, also called a Bragg gap (Joannopoulos, Meade and

Winn [1995]). The intensity-dependent refractive index of the constituent layers allows tuning the properties of the photonic bandgap structure, resulting in optical switching, hysteresis, and bistability. Also, in the nonlinear regime, nonlinearity combined with a strong dispersion owing to the periodic structure may lead to the formation of gap solitons (Winful, Marburger and Garmire [1979], Chen and Mills [1987a], Eggleton, Slusher, de Sterke, Krug and Sipe [1996]). Gap solitons are intense pulses that can propagate inside the photonic bandgap. An important property of gap solitons is their ability to travel at group velocities lower than the speed of light in the medium, making them promising candidates for optical information storage applications.

In addition to a conventional photonic bandgap, a one-dimensional periodic structure consisting of alternating layers of PIM and NIM displays a new type of photonic bandgap, a so-called zero-refractive-index or "zero-n" gap (Li, Zhou, Chan and Sheng [2003]). This new gap is unique to NIM/PIM periodic structures, as it has been shown to exist in a range of frequencies corresponding to a zero (volume) averaged refractive index. The gap due to $\bar{n} = 0$ possesses several unique properties that distinguish it from a Bragg gap: While the Bragg frequency corresponding to the center of the Bragg gap is strongly dependent on the period of the structure (or the lattice constant), the zero-$\bar{n}$ gap is independent of periodicity and remains invariant with the scaling of the lattice constant. In contrast to the Bragg gap, the zero-$\bar{n}$ gap is robust in the presence of the disorder introduced by varying the layer thicknesses and is insensitive to input angle.

In the presence of Kerr nonlinearity, a zero-n gap has been shown to switch from low transmission to a perfectly transmitting state and to form a novel kind of gap soliton (Hegde and Winful [2005a, 2005b]). This zero-n gap soliton has been shown to possess several superior properties in comparison with conventional gap solitons, including relative insensitivity to the angle of incidence and robustness in the presence of structural disorder and material loss. These features significantly simplify the excitation of these new solitons and the realization of their potential practical applications.

Gap solitons have also been predicted even in a single optically thick slab of NIM (D'Aguanno, Mattiucci, Scalora and Bloemer [2004]). The gap in a single slab of NIM originates from the frequency-dependent NIM parameters ε and μ that, for example, can take the form (Ziolkowski and Hayman [2001], D'Aguanno, Mattiucci, Scalora and Bloemer [2004])

$$\varepsilon(\tilde{\omega}) = 1 - \frac{1}{\tilde{\omega}(\tilde{\omega} + \mathrm{i}\tilde{\gamma}_\mathrm{e})}, \qquad \mu(\tilde{\omega}) = 1 - \frac{(\omega_\mathrm{pm}/\omega_\mathrm{pe})^2}{\tilde{\omega}(\tilde{\omega} + \mathrm{i}\tilde{\gamma}_\mathrm{m})}, \tag{5.9}$$

where $\tilde{\omega} = \omega/\omega_\mathrm{pe}$ is the normalized frequency, ω_pe and ω_pm are the respective electric and magnetic plasma frequencies, and $\tilde{\gamma}_\mathrm{e}$ and $\tilde{\gamma}_\mathrm{m}$ are the respective

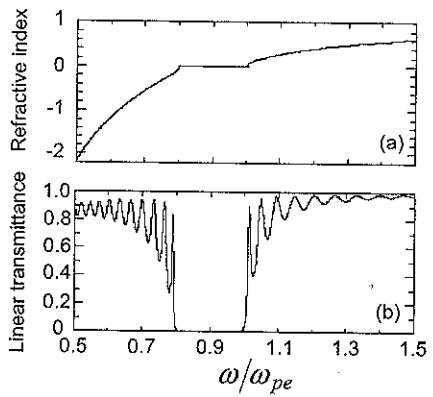

Fig. 17. (a) Refractive index as a function of normalized frequency. (b) Linear transmittance of the NIM slab. (See D'Aguanno, Mattiucci, Scalora and Bloemer [2004].)

normalized electric and magnetic loss terms. Figure 17 shows the frequency-dependent refractive index and linear transmittance of a single nonlinear NIM slab. The spectral width of the gap $\Delta\omega_\mathrm{g}$ and the center-gap frequency ω_gc depend on the electric and magnetic plasma frequency as follows: $\Delta\omega_\mathrm{g} = |\omega_\mathrm{pe} - \omega_\mathrm{pm}|$ and $\omega_\mathrm{gc} = (\omega_\mathrm{pe} + \omega_\mathrm{pm})/2$. While it is expected that a single slab of dispersive material with a cubic nonlinearity supports soliton waves in general, a remarkable feature of the NIM slab is that it supports both bright and dark gap solitons. In the case of self-focusing nonlinearity and $\omega_\mathrm{pm}/\omega_\mathrm{pe} < 1$, bright solitons are excited near the high-frequency edge of the gap where $n > 0$, while dark solitons are excited near the low-frequency edge where $n < 0$.

5.4. *Optical bistability*

Optical bistability is a class of optical phenomena in which a nonlinear system can exhibit two steady transmission states for the same input intensity (Gibbs [1985]). The input–output characteristic of such a system forms a hysteresis loop. Optical bistability has been predicted and experimentally realized in various settings, including a Fabry–Perot resonator filled with a nonlinear material (Gibbs [1976]), layered periodic structures (Winful, Marburger and Garmire [1979]), and a nonlinear slab (Chen and Mills [1987b], Basharov [1988], Trutschel and Lederer [1988], Trutschel, Lederer and Langbein [1989]). A nonlinear film surrounded by a linear dielectric with a high refractive index is known to exhibit bistability and more generally multistability when illuminated at an angle θ_in,

such that $\theta_{res} < \theta_{in} < \theta_{TIR}$, where θ_{res} is the angle corresponding to the resonant peak nearest to the angle of total internal reflection (TIR) θ_{TIR} in the linear transmission curve (Trutschel, Lederer and Langbein [1989]). In this configuration, transmission in the linear regime is low. However, as the incident intensity increases, in the case of self-focusing Kerr nonlinearity, the nonlinear refractive index increases, resulting in a shift of both θ_{TIR} and θ_{res} to larger values. Simultaneously, the transmission coefficient becomes a multi-valued function of the input flux, leading to bistable behavior.

Optical bistability has been predicted and numerically studied in various NIM structures, including symmetric and asymmetric layered periodic structures with multiple NIM layers or a NIM defect (Feise, Shadrivov and Kivshar [2004, 2005], Hegde and Winful [2005b]), a Fabry–Perot resonator containing a nonlinear NIM material (D'Aguanno, Mattiucci, Scalora and Bloemer [2004]).

Since currently optical NIMs are available only in the form of a thin film, the nonlinear transmission properties of a layered structure consisting of a nonlinear slab and a sub-wavelength layer of NIM (with a width similar to the first experimentally demonstrated NIM films) have been investigated (Litchinitser, Gabitov, Maimistov and Shalaev [2007]). It has been shown that even such a thin film of NIM could significantly modify the nonlinear response of such a bilayer. The optical bistability phenomenon in these structures may be used as a novel tool for NIM characterization, owing to the very high sensitivity of the hysteresis width and depth to the changes of the NIM parameters, as shown in fig. 18. In addition, nonreciprocal transmission with enhanced operational range has been demonstrated numerically, enabling novel device applications such as optical memory and the optical diode.

5.5. *Ultra-narrow spatial solitons*

Boardman, Velasco, King and Rapoport [2005] and Boardman, Egan, Velasco and King [2005] have numerically studied interactions of so-called "optical needles" with NIMs. An optical needle is a form of spatial soliton or stable self-channeling with a channel width smaller than the linear wavelength of the light in a medium with a self-focusing nonlinearity. Owing to their extremely high concentration of optical power, optical needles are attractive from both fundamental and applied standpoints.

Figure 19a presents the example of a soliton lens comprised of a slab of linear NIM and a linear PIM, which has been shown to enable the distortionless delivery of an ultranarrow soliton from one nonlinear medium to another through an entirely linear region. This soliton lens is based on the concept of 'complementary

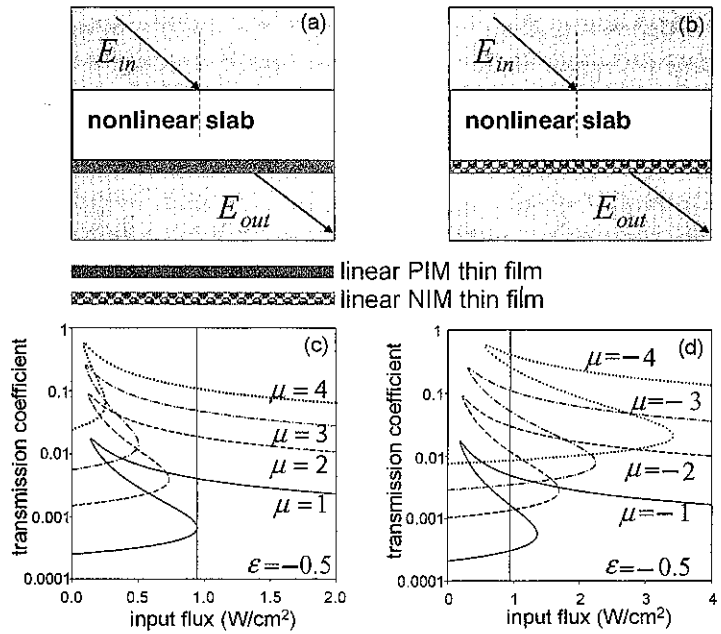

Fig. 18. Schematics of a bilayer structure comprising (a) PIM thin film and (b) NIM thin film. (c,d) Transmission coefficient versus input flux for fixed ε and varying μ of (c) the PIM thin film and (d) the NIM thin film.

media' introduced by Pendry and Ramakrishna [2003], which are known to optically cancel out one another at a specific frequency. The simulation results based on the finite-difference time-domain method illustrating the process of diffraction cancellation in a soliton lens are shown in fig. 19b. The possibility of delivering optical needle-like beams from one point in space to another may be important for the development of future sub-wavelength all-optical chips.

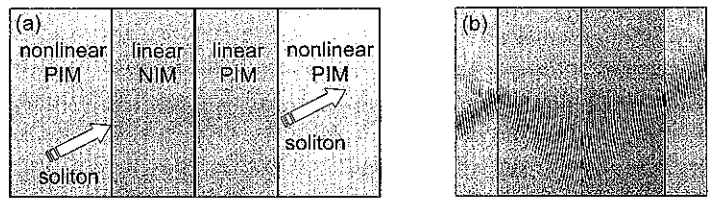

Fig. 19. (a) A soliton lens comprised of a slab of linear NIM and PIM; (b) diffraction cancellation in a soliton lens.

Other novel soliton phenomena predicted in NIMs include single- and multi-hump, symmetric and antisymmetric, and asymmetric spatial solitons (Shadrivov and Kivshar [2005]) and nonlinearity-induced wave transmission through an opaque NIM slab accompanied by the generation of spatiotemporal solitons (Shadrivov, Zharova, Zharov and Kivshar [2005]).

§ 6. "Backward" phase-matching conditions: Implications for nonlinear optics

Wave mixing represents one of the most general and important processes in nonlinear optics. If two electromagnetic waves with carrier frequencies ω_1 and ω_2 propagate in a quadratic nonlinear medium characterized by a nonlinear (electric) susceptibility $\chi_p^{(2)}$, a number of new frequencies can be generated, including $\omega_1 \pm \omega_2$ (sum- and difference-frequency generation), $2\omega_1$ and $2\omega_2$ (second-harmonic generation, SHG). However, the relative efficiency of these processes varies in dispersive media. The so-called phase-matching condition determines which process dominates.

The equations describing the three wave interactions in a $\chi^{(2)}$-medium in the slowly varying envelope and phase approximation can be written in the following form (Shen [1984]):

$$\left(\hat{k}_1\frac{\partial}{\partial z}+\frac{1}{v_1}\frac{\partial}{\partial t}\right)A_1 = \mathrm{i}\frac{2\pi\omega_1^2\mu(\omega_1)}{c^2k_1}P^{\mathrm{NL}}(\omega_1)\exp(-\mathrm{i}k_1z),$$
$$\left(\hat{k}_2\frac{\partial}{\partial z}+\frac{1}{v_2}\frac{\partial}{\partial t}\right)A_2 = \mathrm{i}\frac{2\pi\omega_2^2\mu(\omega_2)}{c^2k_2}P^{\mathrm{NL}}(\omega_2)\exp(-\mathrm{i}k_2z),$$
$$\left(\hat{k}_3\frac{\partial}{\partial z}+\frac{1}{v_3}\frac{\partial}{\partial t}\right)A_3 = \mathrm{i}\frac{2\pi\omega_3^2\mu(\omega_3)}{c^2k_3}P^{\mathrm{NL}}(\omega_3)\exp(-\mathrm{i}k_3z), \qquad (6.1)$$

where $k_j^2 = (\omega_j/c)^2\varepsilon(\omega_j)\mu(\omega_j)$, $\hat{k}_j$ is the sign of $\sqrt{\varepsilon(\omega_j)\mu(\omega_j)}$, $n_j^2 = \varepsilon(\omega_j)\mu(\omega_j)$ is the refractive index squared, and

$$P^{\mathrm{NL}}(\omega_1) = \chi^{(2)}(\omega_1;\omega_3,-\omega_2)A_3A_2^*\exp\bigl[\mathrm{i}z(k_3-k_2)\bigr],$$
$$P^{\mathrm{NL}}(\omega_2) = \chi^{(2)}(\omega_2;\omega_3,-\omega_1)A_3A_1^*\exp\bigl[\mathrm{i}z(k_3-k_1)\bigr],$$
$$P^{\mathrm{NL}}(\omega_3) = \chi^{(2)}(\omega_3;\omega_1,\omega_2)A_1A_2\exp\bigl[\mathrm{i}z(k_1+k_2)\bigr]. \qquad (6.2)$$

The right-hand sides of eqs. (6.1) are not affected by the signs of ε and μ; however, the direction of wave propagation is defined by the sign of $\sqrt{\varepsilon(\omega_j)\mu(\omega_j)}$. Equations (6.1) describe the process of SHG if $\omega_1 = \omega_2 \equiv \omega$, $A_1 \equiv A_2 \equiv A_\omega$ are the frequency and the amplitude of the fundamental wave, and $\omega_3 = 2\omega_1 \equiv 2\omega$, $A_3 \equiv A_{2\omega}$ are the frequency and the amplitude of the second harmonic. The process of parametric amplification is described by eqs. (6.1) if $\omega_1 \equiv \omega_s$, $A_1 \equiv A_s$ correspond to the frequency and the amplitude of the signal wave, $\omega_2 = \omega_i$, $A_2 \equiv A_i$ are those of the idler wave, and $\omega_3 = \omega_p$, $A_3 \equiv A_p$ correspond to the pump wave. Also, it is convenient to re-define $\varepsilon(\omega_j) \equiv \varepsilon_j$ and $\mu(\omega_j) \equiv \mu_j$.

6.1. Second-harmonic generation

Second-harmonic generation is a nonlinear process, in which photons at fundamental frequency ω interacting with a nonlinear material are combined to create new photons with a doubled ("second harmonic") frequency 2ω.

In NIMs fundamentally new regimes of SHG can be realized owing to the inherent frequency dependence of material properties and their unique property of antiparallel phase and energy velocity directions (Zharov, Zharova, Shadrivov and Kivshar [2005], Popov and Shalaev [2006a], Popov, Slabko and Shalaev [2006], Shadrivov, Zharov and Kivshar [2006]). Note that the SHG process is considered here for the case of nonlinear polarization instead of that of nonlinear magnetization, as in Shadrivov, Zharov and Kivshar [2006], and Popov and Shalaev [2006a], in order to compare to the conventional case of SHG in PIMs. The equations for the electric and magnetic field components are very similar, with the exception that the factor $\varepsilon(\omega)$ entering the equations for the magnetic field is replaced by the factor $\mu(\omega)$ when the equations are re-written for the electric field.

Figure 20a shows a schematic of the SHG process in a NIM slab. It is assumed that the material is a NIM at the fundamental frequency ω and it is a PIM at the second-harmonic frequency 2ω. The energy flow of the fundamental frequency is assumed to be from left to right. Since in NIMs the directions of the Poynting vector (energy flow) and the phase velocity are opposite, the phase of the wave at the fundamental frequency travels from right to left. In order to satisfy the phase-matching requirement $k_{2\omega} = 2k_\omega$, the k-vector of the generated second harmonic should also travel from right to left. Since the second harmonic propagates in the PIM, its energy flow is co-directed with the phase velocity and, therefore, the energy propagates from right to left as well, as shown in fig. 20a. This new type of phase-matching condition, "backward phase-matching", has been shown to enable a fundamentally new SHG regime. For comparison a schematic of the SHG process in a PIM is shown in fig. 20b.

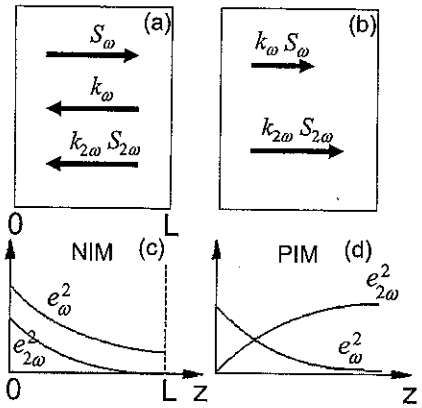

Fig. 20. (a,b) Schematic of the SHG process in (a) NIMs and (b) PIMs. (c,d) Fundamental and second-harmonic field amplitudes squared versus z in (c) NIMs and (d) PIMs. (Adapted from Popov and Shalaev [2006a].)

For SHG in a NIM eqs. (6.1) take the form

$$\left(-\frac{\partial}{\partial z}+\frac{1}{v_\omega}\frac{\partial}{\partial t}\right)A_\omega = \mathrm{i}\frac{2\pi\omega^2\mu_\omega}{c^2k_\omega}P^{\mathrm{NL}}(\omega)\exp(-\mathrm{i}k_\omega z),$$
$$\left(\frac{\partial}{\partial z}+\frac{1}{v_{2\omega}}\frac{\partial}{\partial t}\right)A_{2\omega} = \mathrm{i}\frac{2\pi(2\omega)^2\mu_{2\omega}}{c^2k_{2\omega}}P^{\mathrm{NL}}(2\omega)\exp(-\mathrm{i}k_{2\omega}z). \qquad (6.3)$$

Assuming the continuous-wave case and using the symmetry properties of the tensor $\chi^{(2)}$ (Shen [1984], Boyd [1992]), eqs. (6.3) can be written in the form

$$\frac{\partial A_\omega}{\partial z} = -\mathrm{i}\frac{2K\omega^2\mu_\omega}{c^2k_\omega}A_{2\omega}A_\omega^*\exp[-\mathrm{i}\Delta kz],$$
$$\frac{\partial A_{2\omega}}{\partial z} = \mathrm{i}\frac{4K\omega^2\mu_{2\omega}}{c^2k_{2\omega}}A_\omega^2\exp[\mathrm{i}\Delta kz], \qquad (6.4)$$

where $\Delta k = 2k_\omega - k_{2\omega}$, $K = \frac{2\pi}{c^2}\chi^{(2)}(2\omega) = \frac{\pi}{c^2}\chi^{(2)}(\omega)$,

$$\frac{k_\omega}{\mu_\omega}\frac{\mathrm{d}|A_\omega|^2}{\mathrm{d}z} - \frac{k_{2\omega}}{2\mu_{2\omega}}\frac{\mathrm{d}|A_{2\omega}|^2}{\mathrm{d}z} = 0, \qquad (6.5)$$

or for the energy flow

$$\frac{\mathrm{d}|S_\omega|}{\mathrm{d}z} - \frac{\mathrm{d}|S_{2\omega}|}{\mathrm{d}z} = 0. \qquad (6.6)$$

Assuming that the phase-matching condition $k_{2\omega} = 2k_\omega$ is satisfied (implying that $\varepsilon_\omega = -\varepsilon_{2\omega}$ and $\mu_\omega = -\mu_{2\omega}$), the spatially invariant Manley–Rowe relations take

the form

$$|A_\omega|^2 - |A_{2\omega}|^2 = C^2 = \text{const}. \qquad (6.7)$$

In the conventional PIM case, the Manley–Rowe relations require that the sum of the squared amplitudes is constant. The unusual form of the Manley–Rowe relations in NIMs is explained by the fact that the Poynting vectors for the fundamental and the second harmonic are antiparallel, while their wavevectors are parallel.

The equations for the real amplitudes and phases, introduced as $A_{\omega,2\omega} = e_{\omega,2\omega}\exp(\mathrm{i}\varphi_{\omega,2\omega})$, take the form

$$\frac{\mathrm{d}e_\omega}{\mathrm{d}z} = \kappa e_\omega e_{2\omega}\sin(\theta), \qquad \frac{\mathrm{d}e_{2\omega}}{\mathrm{d}z} = \kappa e_\omega^2\sin(\theta),$$
$$\frac{\mathrm{d}\varphi_\omega}{\mathrm{d}z} = -\kappa e_{2\omega}\cos(\theta), \qquad \frac{\mathrm{d}\varphi_{2\omega}}{\mathrm{d}z} = \kappa\frac{e_\omega^2}{e_{2\omega}}\cos(\theta), \qquad (6.8)$$

where $\theta = \varphi_{2\omega} - 2\varphi_\omega$, $\kappa = 4K\omega^2\mu_{2\omega}/(c^2k_{2\omega})$. Taking into account the equations for φ_ω and $\varphi_{2\omega}$, it is found that $\theta = 3\pi/2$. Then,

$$\frac{\mathrm{d}e_{2\omega}}{\mathrm{d}z} = -\kappa e_\omega^2 = -\kappa\left[C^2 + e_{2\omega}(z)^2\right]. \qquad (6.9)$$

Note that in the PIM case the right-hand sides of eqs. (6.8) for the amplitudes would have opposite signs, while in the case of NIMs the signs are the same. Also, the boundary conditions in the NIM case are specified at opposite interfaces of the slab of a finite length L and are given by $e_\omega(0) = e_{10}$ and $e_{2\omega}(L) = 0$, while in PIMs both conditions are specified at the front interface and are given by $e_\omega(0) = e_{10}$, $e_{2\omega}(0) = 0$. Then, the solutions for $e_{\omega,2\omega}$ in a lossless NIM slab of length L are obtained in the form

$$e_\omega(z) = \frac{C}{\cos[C\kappa(L-z)]}, \qquad e_{2\omega}(z) = C\tan\left[C\kappa(L-z)\right], \qquad (6.10)$$

where

$$C\kappa L = \arccos(C/e_{10}). \qquad (6.11)$$

Therefore, the spatially invariant intensity difference given by eq. (6.7) depends on the slab thickness. Equation (6.7) shows that the incoming radiation at the fundamental frequency can be converted to the second harmonic frequency propagating in the opposite direction with an efficiency approaching 100% in a semi-infinite lossless NIM slab. Thus, the NIM slab acts as a nonlinear mirror. Owing to the boundary conditions for the second harmonic at the rear interface of the slab, the conversion at any point within the NIM slab depends on the total thickness of

the slab. In contrast, in the PIM case the solutions for $e_{\omega,2\omega}$ are

$$e_\omega(z) = \frac{C}{\cosh\left(\frac{z}{z_0}\right)}, \qquad e_{2\omega}(z) = C \cdot \tanh\left(\frac{z}{z_0}\right),$$
$$\text{where } C = e_{10},\ z_0 = \frac{1}{ke_{10}}. \tag{6.12}$$

Figures 20c and d compare the solutions for the NIM and PIM cases.

Another unusual case of SHG in NIMs is realized when the second-harmonic wave corresponds to the NIM's transparent spectral region, while the fundamental wave belongs to the opaque spectral region (Agranovich, Shen, Baughman and Zakhidov [2004a], Zharov, Zharova, Shadrivov and Kivshar [2005]). While the fundamental wave does not propagate in such a metamaterial slab, the material is transparent for the second harmonic frequency. It has been shown that this slab may operate as a nonlinear lens that would provide an image of the source at the second harmonic with sub-wavelength resolution and, therefore, provides an additional means of loss mitigation in NIMs (Zharov, Zharova, Shadrivov and Kivshar [2005]).

SHG in NIMs has also been studied in cavity environments such as a Bragg grating made of alternating NIM/PIM layers (D'Aguanno, Mattiucci, Bloemer and Scalora [2006]). Improved conversion efficiencies, owing to the presence of NIM layers, have been predicted. Finally, Maimistov, Gabitov and Kazantseva [2007] have considered the steady-state propagation of coupled wave packets in the quadratic nonlinear NIM and have found that under some conditions self-trapping of the interacting wave packets takes place. As a result, a two-frequency wave packet (simulton) can be generated with distinct properties as compared with those of solitons in quadratic nonlinear PIMs.

6.2. *Optical parametric amplification*

The backward phase-matching condition has been shown to have a profound effect on the parametric interactions in NIMs. Figures 21a,b show schematics of optical parametric amplification processes in NIMs and PIMs. Assuming that the pump ω_3 and idler ω_2 frequencies belong to the PIM range and the signal ω_1 frequency belongs to the NIM range in undepleted pump approximation, i.e. $A_3 = A_p = \text{const}$, eqs. (6.1) can be written as follows:

$$\frac{dA_1}{dz} = -i\frac{4\pi\omega_1^2\chi^{(2)}\mu_1}{c^2k_1}A_3A_2^*\exp(i\Delta kz),$$
$$\frac{dA_2}{dz} = i\frac{4\pi\omega_2^2\chi^{(2)}\mu_2}{c^2k_2}A_3A_1^*\exp(i\Delta kz), \tag{6.13}$$

where $\Delta k = k_3 - k_1 - k_2$, $\omega_2 = \omega_3 - \omega_1$.

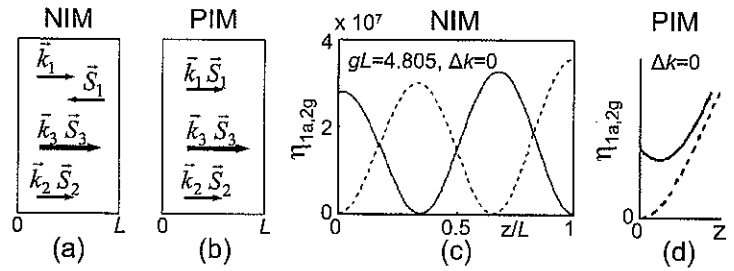

Fig. 21. (a,b) Schematics of optical parametric amplification in (a) NIMs and (b) PIMs. (c,d) The phase-matched amplification factor for the signal wave, and the conversion factor for the idler wave in (c) NIM and (d) PIM with absorption ($\alpha_1 L = 1$, $\alpha_2 L = 1/2$); (d) represents the dependence schematically. (Adapted from Popov and Shalaev [2006b]).

Since loss is one of the major problems in existing NIMs, and especially in those operating at optical frequencies, optical parametric amplification has been proposed as a means to overcome dissipative losses (Popov and Shalaev [2006a]). Then, eqs. (6.13) can be re-written to include the effect of losses α_1 and α_2 as

$$\frac{da_1}{dz} = -iga_2^*\exp(i\Delta kz) + \frac{\alpha_1}{2}a_1,$$
$$\frac{da_2}{dz} = iga_1^*\exp(i\Delta kz) - \frac{\alpha_2}{2}a_2, \tag{6.14}$$

where

$$a_j = \sqrt[4]{\frac{\varepsilon_j}{\mu_j}}\frac{A_j}{\sqrt{\omega_j}} \quad \text{and} \quad g = \frac{4\pi}{c}\chi^{(2)}A_3\frac{\sqrt{\omega_1\omega_2}}{\sqrt[4]{\varepsilon_1\varepsilon_2/\mu_1\mu_2}}.$$

Note that the boundary conditions for a_1 are defined at the opposite side of the slab (of thickness L), as compared with a_2 and are given by $a_1(L) = a_{1L}$ and $a_2(0) = a_{20}$. With these boundary conditions, the solutions to eqs. (6.14) take the form (Popov and Shalaev [2006a, 2006b])

$$a_1(z) = C_1\exp(\beta_1^+ z) + C_2\exp(\beta_2^+ z),$$
$$a_2^*(z) = \kappa_1 C_1\exp(\beta_1^- z) + \kappa_2 C_2\exp(\beta_2^- z), \tag{6.15}$$

where

$$\beta_{1,2}^\pm = \beta_{1,2} \pm \frac{i\Delta k}{2}, \qquad \beta_{1,2} = \frac{\alpha_1 - \alpha_2}{4} + iR,$$
$$C_{1,2} = \pm\frac{a_{1L}\kappa_{2,1} - a_{20}^*\exp(\beta_{2,1}^+ L)}{D},$$
$$D = \kappa_2\exp(\beta_1^+ L) - \kappa_1\exp(\beta_2^+ L), \qquad \kappa_{1,2} = \frac{(\pm R + is)}{g},$$

$$R = \sqrt{g^2 - s^2}, \qquad s = \frac{\alpha_1 + \alpha_2}{4} - \frac{i\Delta k}{2}.$$

Solutions (6.15) describe several unusual properties of parametric amplification in NIMs. In particular, the amplification factor for the signal wave and the conversion efficiency for the idler wave show oscillatory behavior even at $\Delta k = 0$, which is in sharp contrast to those in PIM as illustrated in figs. 21c and d. The reason for this behavior is that the signal and the idler are determined by the boundary conditions on opposite sides of the slab and they increase in opposite directions. Recently, parametric amplification has been demonstrated experimentally in negative-index nonlinear transmission line media (Kozyrev, Kim and van der Weide [2006]). Finally, it is also noteworthy that the possibility of oscillations without a cavity has been found under certain conditions in the NIM slab geometry considered in this section (Popov and Shalaev [2006b]).

§ 7. Surface polaritons, waveguides and resonators

Most of the fascinating properties of NIMs reveal themselves when NIMs are combined with PIMs either in the frequency domain, as discussed in the preceding section, or in the spatial domain. A number of new surface and waveguiding phenomena have been predicted for NIMs and PIMs combined spatially. For example, surface waves (or surface plasmons) are responsible for the improved resolution of a superlens as discussed above. Therefore, a detailed analysis of their properties is of paramount importance.

7.1. Linear surface polaritons

A number of unique and fascinating properties of NIM-based guiding structures have been discovered by Ruppin [2000], Darmanyan, Neviere and Zakhidov [2003, 2005], Shadrivov, Sukhorukov, Kivshar, Zharov, Boardman and Egan [2004], and Boardman, Egan, Velasco and King [2005], Boardman, Velasco, King and Rapoport [2005], D'Aguanno, Mattiucci, Scalora and Bloemer [2005]. Surface polaritons, first predicted by Sommerfeld [1909], are electromagnetic waves propagating along the interface between two media, such that their amplitudes decay exponentially away from the interface. In this subsection both media are assumed to be linear and isotropic, with material parameters (ε_1, μ_1) and (ε_2, μ_2) that can be either positive or negative. The dispersion relation for the TM (TE) type of surface polaritons can be obtained from the solution of the wave equation

for the y component of the magnetic (electric) field

$$\frac{\partial^2 H_y}{\partial z^2} + \frac{\partial^2 H_y}{\partial x^2} + k_0^2 \varepsilon\mu H_y = 0 \quad \text{for the TM wave,}$$
$$\frac{\partial^2 E_y}{\partial z^2} + \frac{\partial^2 E_y}{\partial x^2} + k_0^2 \varepsilon\mu E_y = 0 \quad \text{for the TE wave,} \tag{7.1}$$

where $k_0 = \omega/c$, ω is the wave frequency, c is the speed of light in vacuum, $\varepsilon = \varepsilon_1$, $\mu = \mu_1$ for $x < 0$ and $\varepsilon = \varepsilon_2$, $\mu = \mu_2$ for $x > 0$.

Surface polariton solutions of eqs. (7.1) can be written as

$$H_y = A_0 \exp\bigl(i\beta z - \kappa_{1,2}|x|\bigr), \qquad E_y = A_0 \exp\bigl(i\beta z - \kappa_{1,2}|x|\bigr), \tag{7.2}$$

where A_0 is the wave amplitude at the interface, β is the propagation constant, and $\kappa_{1,2} = [\beta^2 - \varepsilon_{1,2}\mu_{1,2}k_0^2]^{1/2}$ are the transverse wave numbers. The dispersion relations for the two types of surface polaritons are obtained from the requirement that the tangential components of the fields should change continuously across the interface (Ruppin [2000])

$$\kappa_1\varepsilon_2 + \kappa_2\varepsilon_1 = 0 \quad \text{for the TM wave,}$$
$$\kappa_1\mu_2 + \kappa_2\mu_1 = 0 \quad \text{for the TE wave.} \tag{7.3}$$

It is assumed here that ε_1, ε_2, μ_1, μ_2 are real, and therefore, κ_1, κ_2 have to be real and positive so that the field amplitudes decay exponentially away from the interface. Then, the following conditions can be found:

$$\beta^2 > \varepsilon_1\mu_1 k_0^2, \ \varepsilon_2\mu_2 k_0^2. \tag{7.4}$$

Following Shadrivov, Sukhorukov, Kivshar, Zharov, Boardman and Egan [2004] the dispersion relations for the two cases can be written as

$$\beta^2 = k_0^2 \frac{\varepsilon_1\varepsilon_2(\varepsilon_2\mu_1 - \varepsilon_1\mu_2)}{(\varepsilon_2^2 - \varepsilon_1^2)} = \varepsilon_1\mu_1 k_0^2 \frac{X(X-Y)}{(X^2-1)} \quad \text{for the TM case,}$$
$$\beta^2 = k_0^2 \frac{\mu_1\mu_2(\varepsilon_1\mu_2 - \varepsilon_2\mu_1)}{(\mu_2^2 - \mu_1^2)} = \varepsilon_1\mu_1 k_0^2 \frac{Y(Y-X)}{(Y^2-1)} \quad \text{for the TE case,} \tag{7.5}$$

where $X = |\varepsilon_2|/\varepsilon_1$ and $Y = |\mu_2|/\mu_1$. Equations (7.5) define the existence conditions for the surface polaritons. Equations (7.3) and (7.5) for the TM case reduce to the well-known dispersion relation for surface polaritons in conventional materials if both media are non-magnetic. The existence of a TM surface polariton at a PIM/PIM interface requires negative dielectric permeability in one of the semi-infinite media. A TE surface polariton is not supported on such interface of two non-magnetic materials. The existence of a TE surface polariton at a PIM/PIM interface requires negative magnetic permeability on one side of the interface. As

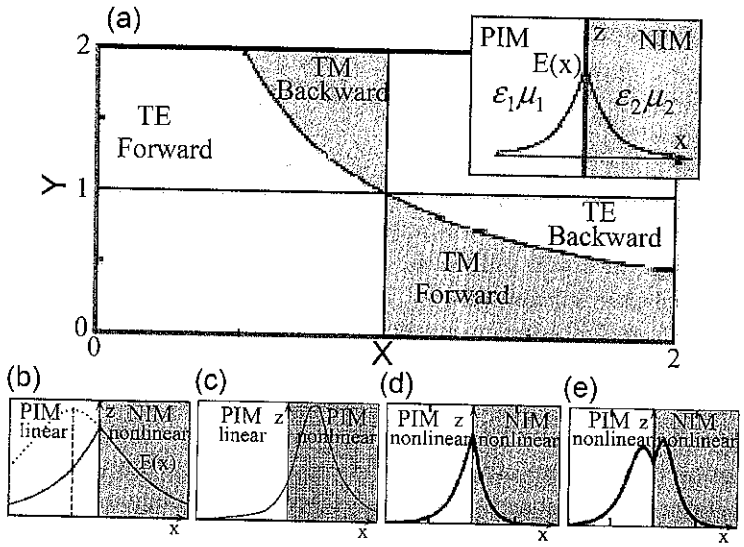

Fig. 22. (a) Existence regions of surface waves on the parameters X and Y. The inset shows the schematics of the geometry and surface wave profile. (b–e) Surface wave profiles for interfaces of different combinations of linear/nonlinear NIMs/PIMs.

until recently negative-ε materials were available but negative-μ materials were not, most studies addressed the TM case only. A TE surface polariton at the interface of two conventional dielectrics has been shown to occur only if at least one of these materials is nonlinear (Litvak and Mironov [1968]).

The existence conditions for surface polaritons that can be supported by a NIM/PIM interface are more complex. One distinctive property of a NIM/PIM interface in comparison with a regular PIM/PIM interface is that both TM and TE surface polaritons can be supported by the same interface in the linear regime, although not simultaneously (i.e. not for the same set of parameters as shown in fig. 22a). However, since a fundamental property of NIMs is the frequency dependence of their material parameters, TE and TM polaritons can exist at different frequencies.

Finally, the energy fluxes in the PIM and NIM half-spaces are given by (Shadrivov, Sukhorukov, Kivshar, Zharov, Boardman and Egan [2004])

$$P = \frac{A_0^2 c^2 \beta}{16\pi\omega\kappa_1} \begin{cases} 1/\varepsilon_1 & \text{for TM,} \\ 1/\mu_1 & \text{for TE,} \end{cases} \quad \text{if } x < 0,$$

$$P = \frac{A_0^2 c^2 \beta}{16\pi\omega\kappa_2} \begin{cases} 1/\varepsilon_2 & \text{for TM,} \\ 1/\mu_2 & \text{for TE,} \end{cases} \quad \text{if } x > 0. \tag{7.6}$$

Equations (7.6) show that if ε_1, $\mu_1 > 0$ and ε_2, $\mu_2 < 0$ the energy fluxes are in opposite directions at the NIM and PIM sides of the interface. *This vortex-like behavior is another unique feature of a linear NIM/PIM interface.* Depending on the material parameters $\varepsilon_{1,2}$ and $\mu_{1,2}$ (or equivalently depending on the relative parameters X and Y) the total energy flux along the interface can be positive (forward waves) or negative (backward waves) as indicated in fig. 22a.

7.2. *Nonlinear surface polaritons*

Nonlinear optics of surface polaritons have been extensively studied at conventional PIM/PIM interfaces for various system configurations. Second-harmonic generation, difference-frequency generation and nonlinear wave-mixing processes are examples of the nonlinear surface effects that have been observed, and they have found numerous applications in the field of surface spectroscopy (Shen [1984]).

A number of unique features of nonlinear surface polaritons have been discovered to exist at a NIM/PIM interface, provided that one or both materials are nonlinear (Shadrivov, Sukhorukov, Kivshar, Zharov, Boardman and Egan [2004]). As an example, in this subsection we examine in detail the properties of TE-polarized surface polaritons at the interface of a nonlinear NIM and a linear PIM.

The material parameters are given by

$$\varepsilon = \begin{cases} \varepsilon_1 & \text{for } x < 0, \\ \varepsilon_2 + \varepsilon_{\mathrm{NL}}|E|^2 & \text{for } x > 0, \end{cases} \quad \text{and} \quad \mu = \begin{cases} \mu_1 & \text{for } x < 0, \\ \mu_2 & \text{for } x > 0. \end{cases} \tag{7.7}$$

Equation (7.1) for the TE case can be re-written as

$$\begin{aligned} &\frac{\partial^2 E}{\partial z^2} + \frac{\partial^2 E}{\partial x^2} + k_0^2 \varepsilon_1 \mu_1 E = 0 && \text{for } x < 0, \\ &\frac{\partial^2 E}{\partial z^2} + \frac{\partial^2 E}{\partial x^2} + k_0^2 \left(\varepsilon_2 \mu_2 + \mu_2 \varepsilon_{\mathrm{NL}} |E|^2\right) E = 0 && \text{for } x > 0. \end{aligned} \tag{7.8}$$

For the case of self-focusing NIM $\mu_2\varepsilon_{\mathrm{NL}} > 0$, the stationary solutions can be searched for in the form $E_{1,2} = \Phi_{1,2}\exp(\mathrm{i}\beta z)$. Then, the transverse profile of the stationary surface polariton is given by

$$\Phi(x) = \begin{cases} E_0 \exp(\eta_1 x) & x < 0, \\ (2/\mu_2\varepsilon_{\mathrm{NL}})^{1/2} \eta_2 \operatorname{sech}[\eta_2 (x - x_0)] & x > 0, \end{cases} \tag{7.9}$$

where E_0 and x_0 are parameters that can be determined from the continuity conditions for the tangential components of the fields at the boundary between the two media. Then, the dispersion relation and the relationship between the electric

field amplitude at the interface and the position of the center of x_0 of the sech function are found in the form

$$\tanh(\eta_2 x_0) = \mu_2\eta_1/(\mu_1\eta_2),$$
$$E_0 = (2/\mu_2\varepsilon_{\rm NL})^{1/2}\eta_2\,\mathrm{sech}(\eta_2 x_0). \tag{7.10}$$

Note that a surface polariton always has a maximum at the interface of a nonlinear NIM and a linear PIM, as shown in fig. 22b, which contrasts with the case of a nonlinear/linear PIM/PIM interface where the electric field has a maximum shifted to the self-focusing nonlinear medium, as shown in fig. 22c (Boardman, Velasco, King and Rapoport [2005]). It can be shown that the same result is obtained in the case of surface polaritons at the interface between a linear NIM and a nonlinear PIM. Figures 22d and e show the structure of the surface polaritons propagating along the nonlinear NIM/nonlinear PIM interface. In this case, depending on the material parameters, the polariton profile consists of either one or two maxima.

Finally, analysis of surface polaritons of finite spatial and temporal extent indicates that the group velocity of nonlinear surface waves can be controlled by changing the intensity of the electromagnetic field. This property provides a new way for manipulating energy flow in such structures, in particular allowing the switching of the surface wave from forward-propagating to backward-propagating. The possibility of controlling surface waves is particularly important for imaging applications based on NIM flat lenses.

7.3. NIM slab as a linear waveguide

The linear properties of guided waves in the NIM slab configuration can be studied using the standard approaches developed for asymmetric or symmetric waveguides (Marcuse [1991]). The dispersion relations for the TE-polarized waves propagating in an asymmetric waveguide described by

$$\begin{cases} \varepsilon_1 > 0,\ \mu_1 > 0 & \text{for } x < 0, \\ \varepsilon_2 < 0,\ \mu_2 < 0 & \text{for } 0 < x < L, \\ \varepsilon_3 > 0,\ \mu_3 > 0 & \text{for } x > 0, \end{cases} \tag{7.11}$$

can be derived as follows. The electric fields that satisfy the linear wave equation (7.1) in each layer can be written as $E_{1,2,3} = \Phi_{1,2,3}\exp(\mathrm{i}\beta z)$. Then, the solutions in the cladding layers, i.e. for $x < 0$ and $x > 0$, are given by

$$\Phi_1(x) = A_1\exp(\kappa_1 x) \quad \text{and} \quad \Phi_3(x) = A_3\exp(-\kappa_3 x),$$

respectively, where $\kappa_1^2 = \beta^2 - k_0^2\varepsilon_1\mu_1 > 0$, $\kappa_3^2 = \beta^2 - k_0^2\varepsilon_3\mu_3 > 0$, with $\kappa_1, \kappa_3 > 0$. In the core layer, i.e. for $0 < x < L$, two cases should be considered:

$$\kappa_2^2 = \beta^2 - k_0^2\varepsilon_2\mu_2 > 0 \quad \text{and} \quad \kappa_2^2 = \beta^2 - k_0^2\varepsilon_2\mu_2 < 0.$$

The former case corresponds to the surface polaritons discussed by Ruppin [2001], also referred to as "slow waves" by Shadrivov, Sukhorukov and Kivshar [2003a], while the latter case corresponds to the slab or "fast" waves. Note that both types of waves are guided waves in the case of NIMs. The solution is given by $\Phi_2(x) = A_2\exp(-\kappa_2 x) + B_2\exp(\kappa_2 x)$. The corresponding dispersion relation is found in the form

$$\left(1 - \frac{\mu_3\kappa_2}{\mu_2\kappa_3}\right)\left(1 - \frac{\mu_2\kappa_1}{\mu_1\kappa_2}\right)\exp(-\kappa_2 L) + \left(1 + \frac{\mu_3\kappa_2}{\mu_2\kappa_3}\right)\left(1 + \frac{\mu_2\kappa_1}{\mu_1\kappa_2}\right)\exp(\kappa_2 L) = 0, \tag{7.12}$$

which reduces to the results of Ruppin [2001] for the symmetric case $\varepsilon_1 = \varepsilon_3 > 0$, $\mu_1 = \mu_3 > 0$:

$$\kappa_2\mu_3 = -\mu_2\kappa_3\tanh(\kappa_2 h/2), \qquad \kappa_2\mu_3\tanh(\kappa_2 h/2) = -\mu_2\kappa_3. \tag{7.13}$$

The corresponding dispersion relations for a TM-polarized wave propagating in a generalized three-layer waveguide can be written as

$$\left(1 - \frac{\varepsilon_3\kappa_2}{\varepsilon_2\kappa_3}\right)\left(1 - \frac{\varepsilon_2\kappa_1}{\varepsilon_1\kappa_2}\right)\exp(-\kappa_2 L) + \left(1 + \frac{\varepsilon_3\kappa_2}{\varepsilon_2\kappa_3}\right)\left(1 + \frac{\varepsilon_2\kappa_1}{\varepsilon_1\kappa_2}\right)\exp(\kappa_2 L) = 0, \tag{7.14}$$

which in the case of symmetric waveguide reduces to

$$\kappa_2\varepsilon_3 = -\varepsilon_2\kappa_3\tanh(\kappa_2 L/2), \qquad \kappa_2\varepsilon_3\tanh(\kappa_2 L/2) = -\varepsilon_2\kappa_3. \tag{7.15}$$

In conventional non-magnetic dielectric or metallic slab waveguides, with frequency-dependent dielectric permittivity, surface polaritons exist only in the stop band, corresponding to negative permittivity. In magnetic material slabs with constant dielectric permittivity and a frequency-dependent magnetic permeability, surface polaritons also exist in the stop band corresponding to negative permeability. In sharp contrast, a NIM slab supports surface localized modes (slow waves) within the frequency pass band (i.e. they are guided waves) corresponding to simultaneously negative permittivity and permeability.

The solution for the guided waves can be written in the form

$$\Phi_2(x) = A_2\exp(-\mathrm{i}\kappa_2 x) + B_2\exp(\mathrm{i}\kappa_2 x).$$

Therefore, in order to re-write the dispersion relations (7.12)–(7.14) for the guided waves, κ_2 can be re-defined as $\kappa_2 \to i\kappa_2$, leading, for example in the case of the TE-polarized wave, to the following dispersion relation:

$$\left(1-\frac{i\mu_3\kappa_2}{\mu_2\kappa_3}\right)\left(1-\frac{\mu_2\kappa_1}{i\mu_1\kappa_2}\right)\exp(-i\kappa_2 L) + \left(1+\frac{i\mu_3\kappa_2}{\mu_2\kappa_3}\right)\left(1+\frac{\mu_2\kappa_1}{i\mu_1\kappa_2}\right)\exp(i\kappa_2 L) = 0, \tag{7.16}$$

which can be written as $\exp[i(2\kappa_2 h+\varphi_1+\varphi_3)] = 1$, where φ_1 and φ_3 are defined as

$$\left(1+\frac{i\mu_1\kappa_2}{\mu_2\kappa_1}\right)\left(1-\frac{i\mu_1\kappa_2}{i\mu_2\kappa_1}\right)^{-1} \equiv \exp(i\varphi_1) \quad \text{and}$$
$$\left(1+\frac{i\mu_3\kappa_2}{\mu_2\kappa_1}\right)\left(1-\frac{i\mu_3\kappa_2}{i\mu_2\kappa_3}\right)^{-1} \equiv \exp(i\varphi_3). \tag{7.17}$$

As a result, the well-known condition for the guided modes of a linear waveguide is obtained:

$$2\kappa_2 h+\varphi_1+\varphi_3 = 2\pi m, \quad m = 0, 1, 2, \ldots. \tag{7.18}$$

Equation (7.18) implies that the total $2\pi m$-phase shift of the zigzagging wave propagating between the two waveguide boundaries includes a propagation phase shift $2\kappa L$, as well as phase shifts φ_1 and φ_3 owing to the total internal reflection at the interfaces (Tamir [1988], Marcuse [1991]) often referred to as the linear Goos–Hänchen shift (Qing and Chen [2004], Shadrivov, Zharov and Kivshar [2003]). These phase shifts can be re-written as

$$\tan\left(\frac{\varphi_1}{2}\right) = \frac{\mu_1}{\mu_2}\sqrt{\frac{k_0^2\varepsilon_2\mu_2-\beta^2}{\beta^2-k_0^2\varepsilon_1\mu_1}} \quad \text{and} \quad \tan\left(\frac{\varphi_3}{2}\right) = \frac{\mu_3}{\mu_2}\sqrt{\frac{k_0^2\varepsilon_2\mu_2-\beta^2}{\beta^2-k_0^2\varepsilon_3\mu_3}}. \tag{7.19}$$

Equations (7.19) show that in contrast to the conventional PIM/PIM interface, in the case of the NIM/PIM interface the Goos–Hänchen shift possesses a negative sign.

Detailed analysis of the dispersion relations for the symmetric NIM slab has revealed several unusual properties of such waveguides (Shadrivov, Sukhorukov and Kivshar [2003a]), which can be summarized as follows. NIM slab waveguides support slow modes that can be symmetric (node-less) or antisymmetric (containing one zero). In contrast to the conventional PIM waveguides that can only support fast guided modes if the refractive index of the core is higher than that of the cladding, guided modes can be supported by both a low-index

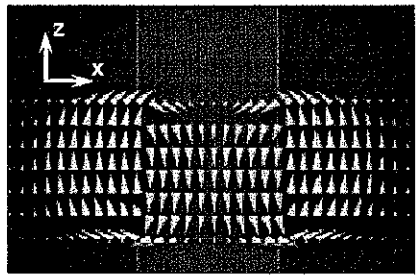

Fig. 23. Double-vortex structure of energy flow for localized surface wave. (See Shadrivov, Sukhorukov and Kivshar [2003a].)

and a high-index NIM slab. The fundamental node-less mode that always exists in PIM slab waveguides does not exist at all in the NIM slab. While PIM waveguides also support higher-order modes with well-defined properties, their number being determined by the so-called V-parameter ($V = (2h/\lambda)\sqrt{n_2^2-n_1^2}$ for a symmetric waveguide), in NIM waveguides the properties of higher-order modes are more complex. For instance, the first-order mode disappears as the waveguide width exceeds some critical value. Also, two modes with the same number of nodes can be simultaneously supported. Finally, as discussed above, the energy fluxes are counter-directed at the interface of the NIM and PIM. Results of numerical simulations indeed show a unique double-vortex structure of the energy flow for the localized surface wave in the NIM slab (fig. 23).

7.4. *Linear waveguide in nonlinear surroundings*

In this subsection we consider a linear NIM slab waveguide surrounded by a nonlinear dielectric. Similar to the linear case discussed above, this waveguide supports bounded surface (slow) waves $\kappa_2^2 = \beta^2 - k_0^2\varepsilon_2\mu_2 > 0$ and slab (fast) modes $\kappa_2^2 = \beta^2 - k_0^2\varepsilon_2\mu_2 < 0$.

The waveguide material parameters are given by

$$\begin{cases} \varepsilon_1 + \varepsilon_{\rm NL}^{(1)} > 0, \ \mu_1 > 0, \\ \varepsilon_2 < 0, \ \mu_2 < 0, \\ \varepsilon_3 + \varepsilon_{\rm NL}^{(3)} > 0, \ \mu_3 > 0. \end{cases} \tag{7.20}$$

For the surface waves the solutions in the slab ($0 < x < L$) are found in the form $\Phi_2(x) = A_2\exp(-\kappa x) + B_2\exp(\kappa x)$. The solutions in the claddings are given

by

$$\Phi_j(x) = \left(\frac{2\kappa_j^2}{k_0^2\mu_j\varepsilon_{\rm NL}^{(j)}}\right)^{-1/2} \operatorname{sech}\big[\kappa_j(x-x_j)\big],$$

$$\text{for } |x| > L \text{ and } \mu_j\varepsilon_{\rm NL}^{(j)} > 0, \tag{7.21}$$

$$\Phi_j(x) = \left(\left|\frac{2\kappa_j^2}{k_0^2\mu_j\varepsilon_{\rm NL}^{(j)}}\right|\right)^{-1/2} \operatorname{cosech}\big[p_j(x-x_j)\big],$$

$$\text{for } |x| > L \text{ and } \mu_j\varepsilon_{\rm NL}^{(j)} < 0, \tag{7.22}$$

where $\kappa_1^2 = \beta^2 - k_0^2\varepsilon_1\mu_1$, $\kappa_3^2 = \beta^2 - k_0^2\varepsilon_3\mu_3$, and x_j are the integration constants corresponding to the maxima of the electric field, $j = 1$ or 3. Depending on the signs of $\mu_j\varepsilon_{\rm NL}^{(j)}$, four solutions are possible. Here, as an example we consider the case of $\mu_j\varepsilon_{\rm NL}^{(j)} > 0$. Then, the dispersion relations are found in the form

$$\exp(2\kappa_2 L)\left(1+\frac{\kappa_1\mu_2}{\kappa_2\mu_1}\tanh(\kappa_1 x_1)\right)\left(1+\frac{\kappa_3\mu_2}{\kappa_2\mu_3}\tanh\big[\kappa_3(L-x_3)\big]\right)$$
$$= \left(1-\frac{\kappa_1\mu_2}{\kappa_2\mu_1}\tanh(\kappa_1 x_1)\right)\left(1-\frac{\kappa_3\mu_2}{\kappa_2\mu_3}\tanh\big[\kappa_3(L-x_3)\big]\right). \tag{7.23}$$

Defining ϕ_1 and ϕ_3 by

$$\tanh(\phi_1/2) = \frac{\kappa_1\mu_2}{\kappa_2\mu_1}\tanh(\kappa_1 x_1),$$
$$\tanh(\phi_3/2) = \frac{\kappa_3\mu_2}{\kappa_2\mu_3}\tanh\big[\kappa_3(L-x_3)\big], \tag{7.24}$$

Equation (7.23) takes the form

$$2\kappa_2 L + \phi_1 + \phi_3 = 0, \tag{7.25}$$

and can be satisfied if either ($\phi_1 < 0$ or $\phi_3 < 0$) or (ϕ_1 and $\phi_3 < 0$).

Finally, if the electric field amplitudes at the interfaces $x = 0$ and $x = L$ are defined as

$$A_{12} = \left(\frac{2\kappa_1^2}{k_0^2\mu_1\varepsilon_{\rm NL}^{(1)}}\right)^{-1/2} \operatorname{sech}\big[\kappa_1(x-x_1)\big] \quad \text{and}$$

$$A_{23} = \left(\frac{2\kappa_3^2}{k_0^2\mu_3\varepsilon_{\rm NL}^{(3)}}\right)^{-1/2} \operatorname{sech}\big[\kappa_3(x-x_3)\big] \tag{7.26}$$

then the relationship between the parameters x_1 and x_3 can be found from

$$A_{23} = A_{12}\big[\cosh(\kappa_2 L) - (\mu_2\kappa_1/\kappa_2)\sinh(\kappa_2 L)\big], \tag{7.27}$$

that is, a relationship between x_1 and x_2. Then the dispersion relation (7.23) contains x_1 as a parameter. On the other hand, eqs. (7.26) determine A_{12} in terms of x_1. Therefore, the electric field amplitude at $x = 0$ can be chosen as a parameter instead of x_1. Then, (7.23) and (7.26) provide an implicit relationship between the propagation constant β and the frequency ω, $\beta = \beta(\omega; A_{12}^2)$.

Corresponding dispersion relations and their analysis for the case of slab (fast) modes have been performed by Shadrivov [2004] and will not be detailed here. In particular, symmetric, asymmetric, and antisymmetric, forward and backward modes have been found.

7.5. Nano-resonators

Optical resonators are the essential components of many optical systems, including lasers, parametric oscillators, interferometers, optical delay lines, and filters. The simplest form of resonator is a plane mirror Fabry–Perot cavity. The resonance condition in a Fabry–Perot cavity of length L is given by $2L = m\lambda$, where m is an integer number and λ is the optical wavelength in the medium filling the resonator. Therefore, the lower limit on the length of the cavity that supports the lowest-order resonant mode is $L = \lambda/2 = \lambda_0/(2n)$, where λ_0 is the optical wavelength in vacuum and n is the index of refraction of the resonator medium. Engheta [2002] has shown that significantly more compact sub-wavelength cavities can be realized using NIM layers inside the resonator.

The dispersion relation for a resonator formed by two perfectly conducting plates filled with two materials of thicknesses d_1 and d_2 with corresponding material parameters (ε_1, μ_1) and (ε_2, μ_2) shown in fig. 24, can be obtained as follows. In layer 1 ($0 \leqslant x \leqslant d_1$), the electric and magnetic field components can be written as

$$E_x^{(1)} = E_0^{(1)}\sin(n_1 k_0 z), \qquad H_y^{(1)} = \frac{n_1 k_0}{\mathrm{i}\omega\mu_1}E_0^{(1)}\cos(n_1 k_0 z), \tag{7.28}$$

and in layer 2 ($d_1 \leqslant x \leqslant d_1 + d_2$) they are given by

$$E_x^{(2)} = E_0^{(2)}\sin\big[n_2 k_0(d_1 + d_2 - z)\big],$$
$$H_y^{(2)} = -\frac{n_2 k_0}{\mathrm{i}\omega\mu_2}E_0^{(2)}\cos\big[n_2 k_0(d_1 + d_2 - z)\big]. \tag{7.29}$$

From the boundary conditions,

$$E_0^{(1)}\sin(n_1 k_0 d_1) = E_0^{(2)}\sin(n_2 k_0 d_2),$$
$$\frac{n_1}{\mu_1}E_0^{(1)}\cos(n_1 k_0 d_1) = -\frac{n_2}{\mu_2}E_0^{(2)}\cos(n_2 k_0 d_2), \tag{7.30}$$

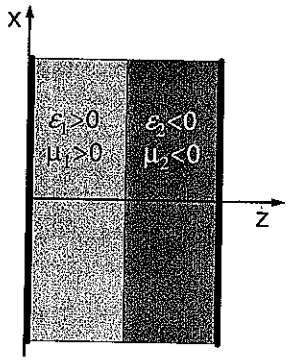

Fig. 24. Sub-wavelength compact cavity resonator formed by a pair of NIM and PIM layers sandwiched between two reflectors. (Adapted from Engheta [2002].)

the dispersion relations are obtained in the form

$$\frac{n_2}{\mu_2}\tan(n_1k_0d_1) + \frac{n_1}{\mu_1}\tan(n_2k_0d_2) = 0. \tag{7.31}$$

Note that up to this point the signs of n_1, n_2, μ_1, and μ_2 have not been specified. Assuming layer 1 is the PIM layer ($\varepsilon_1 > 0$, $\mu_1 > 0$) and layer 2 ($\varepsilon_2 < 0$, $\mu_2 < 0$) is the NIM layer, eq. (7.31) can be re-written as

$$\frac{|n_2|}{|\mu_2|}\tan\big(|n_1|k_0d_1\big) - \frac{n_1}{|\mu_1|}\tan\big(|n_2|k_0d_2\big) = 0, \tag{7.32}$$

which finally leads to

$$\frac{\tan(|n_1|k_0d_1)}{\tan(|n_2|k_0d_2)} = \frac{|\mu_2||n_1|}{|\mu_1||n_2|}. \tag{7.33}$$

Equation (7.33) shows that in this case (PIM/NIM configuration) there are no limitations on the total length of the resonator, i.e. on $L = d_1 + d_2$, but rather on the ratio of d_1 and d_2. This conclusion becomes more obvious if d_1, d_2 and ω are chosen such that the small-argument approximation can be used for the tangent function, in which case eq. (7.33) reduces to

$$\frac{d_1}{d_2} \cong \frac{|\mu_2|}{|\mu_1|}. \tag{7.34}$$

In contrast, if both layers 1 and 2 are made of PIMs (PIM/PIM configuration), eq. (7.31) is still valid, but the tangent functions should have opposite signs in order to satisfy eq. (7.31). Then, if $d_1 < \pi/(2n_1k_0)$ for $\tan(n_1k_0d_1)$ to be positive, d_2 must exceed $\pi/(2n_2k_0)$ in order to have $\tan(n_2k_0d_2)$. As a result, there is a limitation on the total length $L = d_1 + d_2$.

The idea of sub-wavelength cavity resonators based on NIM/PIM pairs has been further extended to the case of ultracompact waveguides (Alu and Engheta [2004]), backward couplers (Engheta and Ziolkowski [2005]) and lasers (Ziolkowski [2006]). The development of such ultrasmall photonic components is essential for future nano- and microphotonic integrated circuits.

§ 8. New frontiers: Metamaterials for cloaking

While the first optical metamaterials were demonstrated only two years ago (Shalaev, Cai, Chettiar, Yuan, Sarychev, Drachev, Kildishev [2005], Zhang, Fan, Panoiu, Malloy, Osgood, Brueck [2005]) numerous potential applications are envisioned. These include nanoscale lithography, biological imaging, beam steering, optical memory, sensing, improved light coupling to solar cells and light out-coupling from organic light-emitting devices and optical nanocomponents, and even the possibility of controlling an object's degree of visibility. Recently, three approaches have been proposed to achieve a nearly perfect shielding effect, or "cloaking": one based on a plasmonic or metamaterial cover proposed by Alu and Engheta [2005a], a superlens-based approach introduced by Milton and Nicorovici [2006], and a coordinate-transformation or wave-redirection approach proposed by Pendry, Schurig and Smith [2006] and independently by Leonhardt [2006]. Of these three approaches, the coordinate-transformation approach appears to be the most general in the following sense: the design of the cloak is not "object-specific", i.e. the same cloak can be used for different objects and, importantly, microscopic as well as macroscopic objects can be made invisible using this approach. The theory behind this approach originates from Ward and Pendry's paper (Ward and Pendry [1996]), where the problem of computational studies of complex systems involving several length scales was addressed. An example of such scales is the wavelength of light in free space, which can be on the order of a few thousand Ångströms, compared to the skin depth in metals, which is usually a few tens of Ångströms. It has been shown that instead of using a non-uniform mesh, the conventional approach to this kind of problem, details of the mesh structure can be included into an effective ε and μ.

With respect to cloaking applications, the idea of coordinate transformation can be utilized as follows. To cloak an object in a certain volume of space, the space should be transformed to create a concealment volume. Since actual space transformation is not feasible, one could use the fact that in Maxwell's equations the material parameters enter in such a way that the same effect can be achieved by transforming the material properties. Therefore, the space outside the conceal-

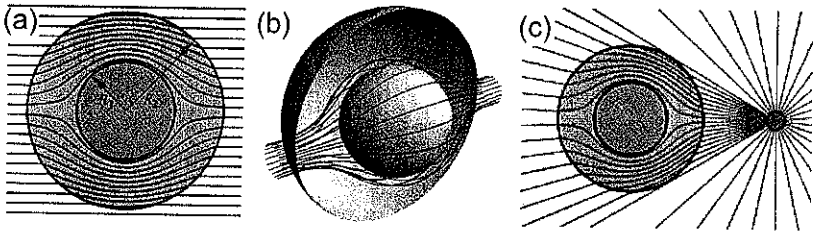

Fig. 25. (a,b) Ray trajectories in the cloak assuming that $R_2 \gg \lambda$: (a) two-dimensional cross section; rays are diverted within the annulus of cloaking material contained within $R_1 < r < R_2$ and return to their original path on the far side of the cloak; (b) three-dimensional view of the same system. (c) A point charge located near the cloaked sphere. (Here it is assumed that $R_2 \ll \lambda$, the near-field limit. The electric displacement field is plotted. The field is excluded from the cloaked region, but emerges on the far side of the cloaking sphere undisturbed.) (Adapted from Pendry, Schurig and Smith [2006].)

ment volume can be replaced by a material in which light rays travel the exact same paths they would have traveled in the transformed space.

Maxwell's equations in a system of Cartesian coordinates are given by

$$\nabla \times E = -\frac{\mu}{c}\frac{\partial H}{\partial t}, \qquad \nabla \times H = \frac{\varepsilon}{c}\frac{\partial E}{\partial t}, \tag{8.1}$$

where both ε and μ may depend on position. Ward and Pendry proved that the transformation to a general system defined as

$$q_1(x, y, z), \quad q_2(x, y, z), \quad q_3(x, y, z) \tag{8.2}$$

does not change the form of Maxwell's equations but changes the definitions of ε and μ (Ward and Pendry [1996], Leonhardt [2003]). Maxwell's equations in the new system of coordinates can be written as

$$\nabla_q \times \hat{E} = -\frac{\hat{\mu}}{c}\frac{\partial \hat{H}}{\partial t}, \qquad \nabla_q \times \hat{H} = \frac{\hat{\varepsilon}}{c}\frac{\partial \hat{E}}{\partial t}, \tag{8.3}$$

where $\hat{\varepsilon}$ and $\hat{\mu}$ are in general tensors, and $\hat{E}$ and $\hat{H}$ are renormalized electric and magnetic fields.

An example of a cloaking device is shown in fig. 25. The object, chosen to be a sphere of radius R_1 for simplicity, is concealed with a metamaterial that is designed to deflect the rays that would have hit the object, guide them around the object, and return them to their original path. The cloaking region is contained within the annulus $R_1 < r < R_2$. A coordinate transformation that takes all fields in the region $r < R_2$ and compresses them into the region $R_1 < r < R_2$ is given by

$$r' = R_1 + r(R_2 - R_1)/R_2, \qquad \theta' = 0, \qquad \phi' = \phi. \tag{8.4}$$

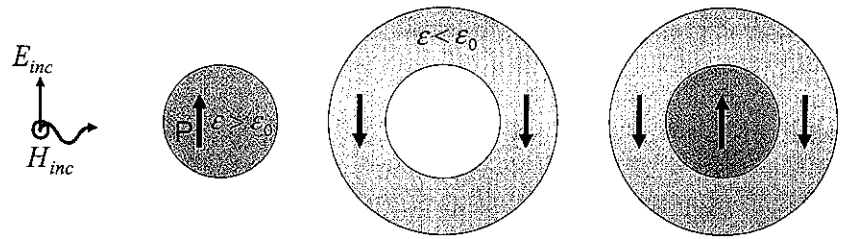

Fig. 26. Cancellation of the overall dipole moment through an induced negative polarization vector. (Adapted from Alu and Engheta [2005a].)

The corresponding values for the electric permittivity ε' and magnetic permeability μ' can take any value in the region $r < R_1$, and are given by

$$\varepsilon'_{r'} = \mu'_{r'} = \frac{R_2}{R_2 - R_1}\frac{(r' - R_1)^2}{r'}, \qquad \varepsilon'_{\theta'} = \mu'_{\theta'} = \frac{R_2}{R_2 - R_1},$$
$$\varepsilon'_{\phi'} = \mu'_{\phi'} = \frac{R_2}{R_2 - R_1}. \tag{8.5}$$

Finally, for $r > R_2$ all components of ε' and μ' are equal to 1. A cloak designed using eqs. (8.4)–(8.5) will exclude all fields from the central region. On the other hand, no fields can leave the region $r < R_1$.

Several issues are associated with a practical realization of such a cloaking device: (1) very large or very small values of ε' and μ' can be difficult to achieve, and thus, cloaking might be imperfect if some values prescribed by eq. (8.5) cannot be realized; (2) in the example considered by Pendry, Schurig and Smith [2006] the effect is only achieved at one frequency. Obviously, broadband cloaking would be desirable for most practical applications.

Two alternative schemes for the cloaking of objects have been discussed by Alu and Engheta [2005b] and by Milton and Nicorovici [2006]. The basic idea of Alu and Engheta is shown schematically in fig. 26. In this scheme the invisibility results from the cancellation of the overall dipole moment through an induced negative polarization vector in the cloaking region. The cloak and the object form a composite such that the total scattering cross-section is reduced. Some of the current limitations of this approach are (1) single-wavelength operation, (2) object size is limited to microscopic objects, and (3) the cloak is object-specific.

Finally, the third approach, proposed by Milton and Nicorovici [2006], relies on the use of a superlens or, more precisely, on the regions of anomalous localized resonance occurring near superlenses. Nicorovici, McPhedran and Milton [1994] have found that a coated cylinder, now called a cylindrical superlens, with a core

of dielectric constant $\varepsilon_c = 1$ and radius r_c and a shell with dielectric constant $\varepsilon_s = -1 + i\varepsilon_s''$ and outer radius r_s, in the limit $\varepsilon_s'' \to 0$ would be invisible to any applied quasistatic transverse magnetic (TM) field. As an extension of that earlier work, Milton and Nicorovici [2006] have recently shown that not only is the lens invisible in this limit, but cylindrical objects are as well, or at least any finite collection of polarizable line dipoles that lie within a certain radius of the cylindrical superlens.

The main idea of this approach is as follows. When the resonant field generated by a polarizable line or point dipole acts back on the polarizable line or point dipole it effectively cancels the field acting on it from outside sources, resulting in cloaking. Cloaking has been proven in the quasistatic limit for finite collections of polarizable line dipoles that all lie within a specific distance from a coated cylinder with a shell permittivity $\varepsilon_{cl} = -\varepsilon_c = -\varepsilon_{ext}$, where ε_c is the core permittivity and ε_{ext} is the permittivity of the surrounding medium. Also, cloaking extends outside the quasistatic regime for a plane-parallel superlens. When a polarizable line dipole is located less than a distance $d/2$ from the lens, where d is the thickness of the lens, it will be cloaked due to the presence of a resonant field in front of the lens.

The first experimental demonstration of cloaking at microwave frequencies has been reported recently (Schurig, Mock, Justice, Cummer, Pendry, Starr and Smith [2006]). In that experiment the object, a copper cylinder, was concealed by a cylindrical cloak built using SRRs positioned with their axes along the radial direction as shown in fig. 27. Two main design parameters of the SRRs, the length of the split and the radius of the corners, shown in the inset in fig. 27, were used to tune the material parameters to those prescribed by the design equations

$$\varepsilon_z' = \left(\frac{b}{b-a}\right)^2, \qquad \mu_r' = \left(\frac{r-a}{r}\right)^2, \qquad \mu_\theta' = 1. \tag{8.6}$$

Experimental results showing the fields impinging on the bare conducting cylinder and the cloaked conducting cylinder are shown in fig. 27. Although the invisibility demonstrated in these experiments is not perfect owing to simplifications made at the design stage, the feasibility of the electromagnetic cloaking mechanism on the basis of metamaterial design has been demonstrated.

Very recently, the first theoretical design of a non-magnetic cloak operating at optical frequencies was proposed by Cai, Chettiar, Kildishev and Shalaev [2007]. It may take some time before optical cloaking becomes a reality due to the more difficult fabrication of metamaterials at optical frequencies, but basic ideas of cloaking are applicable to all frequencies.

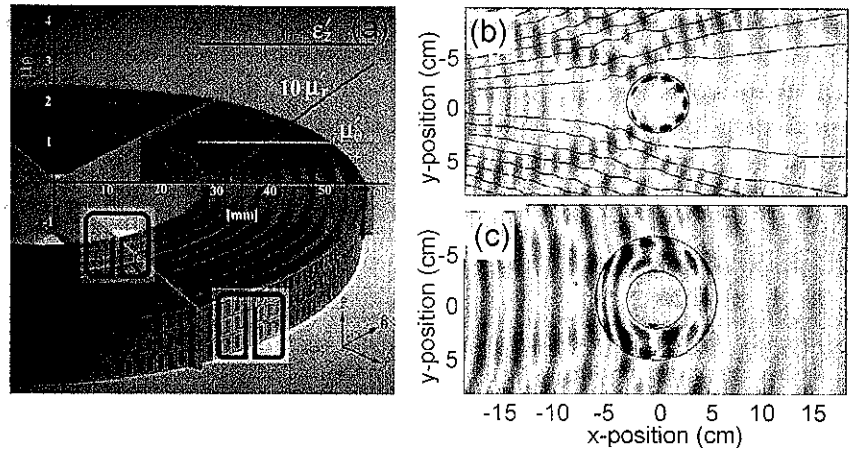

Fig. 27. (a) Two-dimensional experimental cloaking structure. Snapshots of time-dependent, steady-state electric field patterns. The cloak lies in the annular region between two circles and surrounds a conducting Cu cylinder at the inner radius. (b) Experimental measurement of the bare conducting cylinder. (c) Experimental measurement of the cloaked conducting cylinder. (Adapted from Schurig, Mock, Justice, Cummer, Pendry, Starr and Smith [2006].)

§ 9. Summary

The emergence of optical metamaterials, and NIMs in particular, has given rise to numerous unusual linear and nonlinear optical phenomena that cannot be realized in conventional materials. The constituent components of these materials, meta-atoms, can be designed to empower optical magnetic activity, to enable fundamentally new regimes of linear and nonlinear light–matter interaction, and even to manipulate an object's degree of visibility at optical frequencies.

The fabrication of optical NIMs is quite challenging and requires approaches going beyond a straightforward scaling of meta-atom sizes from microwave to near-infrared and visible frequencies. Several proof-of-principle experiments reported over the last two years form the basis for building functional NIMs and the realization of new photonic devices. Nevertheless, there is a lot of room for improvement and, therefore, for both experimental and theoretical fundamental and applied studies. The ultimate goal from the experimental viewpoint is the fabrication of three-dimensional, low-loss, tunable and broadband NIMs. Owing to the complexity of NIMs, theoretical predictions and numerical analysis are the essential components of NIM research.

The demonstration of NIMs and magnetic activity at optical frequencies has motivated re-consideration of almost all well-established linear and nonlinear op-

tical phenomena that reveal themselves in unusual and often counter-intuitive ways in NIMs. Optical metamaterials, without doubt, constitute one of the most exciting areas of research in modern optics, that is likely to result in discoveries of new phenomena and the development of novel device applications for nanophotonics.

Acknowledgements

The authors gratefully acknowledge the support of the Army Research Office through Grants W911NF-07-1-0343 and 50342-PH-MUR, of the National Science Foundation through Grant DMS-050989, and of the Russian Foundation for Basic Research through Grant 06-02-16406.

References

Agranovich, V.M., Gartstein, Yu.N., 2006, Spatial dispersion and negative refraction of light, Usp. Fiz. Nauk **176**, 1051–1068.

Agranovich, V.M., Gartstein, Yu.N., Zakhidov, A.A., 2006, Negative refraction in gyrotropic media, Phys. Rev. B **73**, 045114-12.

Agranovich, V.M., Ginzburg, V.L., 1984, Crystal Optics with Spatial Dispersion, and Excitons, Springer-Verlag, Berlin.

Agranovich, V.M., Shen, Y.R., Baughman, R.H., Zakhidov, A.A., 2004a, Linear and nonlinear wave propagation in negative refraction metamaterials, Phys. Rev. B **69**, 165112-7.

Agranovich, V.M., Shen, Y.R., Baughman, R.H., Zakhidov, A.A., 2004b, Optical bulk and surface waves with negative refraction, J. of Luminescence **110**, 167–173.

Alekseyev, L.V., Narimanov, E., 2006, Slow light and 3D imaging with non-magnetic negative index systems, Opt. Express **14**, 11184–11193.

Alu, A., Engheta, N., 2003, Pairing an epsilon-negative slab with a mu-negative slab: Resonance, tunneling and transparency, IEEE Transactions on Antennas and Propagation **51**, 2558–2571.

Alu, A., Engheta, N., 2004, Guided modes in a waveguide filled with a pair of single-negative (SNG), double-negative (DNG), and/or double-positive (DPS) layers, IEEE Transactions on Microwave Theory and Techniques **52**, 199–210.

Alu, A., Engheta, N., 2005a, Achieving transparency with plasmonic and metamaterial coatings, Phys. Rev. E **72**, 016623-9.

Alu, A., Engheta, N., 2005b, Evanescent growth and tunneling through stacks of frequency-selective surfaces, IEEE Antennas and Wireless Propagation Lett. **4**, 417–420.

Basharov, A.M., 1988, Thin-film of 2-level atoms—A simple-model of optical bistability and self-pulsations, Sov. Phys. JETP **67**, 1741–1744.

Belov, P.A., 2003, Backward waves and negative refraction in uniaxial dielectrics with negative dielectric permittivity along the anisotropy axis, Microwave and Optical Technology Letters **37**, 259–263.

Berrier, A., Mulot, M., Swillo, M., Qiu, M., Thylén, L., Talneau, A., Anand, S., 2004, Negative refraction at infrared wavelengths in a two-dimensional photonic crystal, Phys. Rev. Lett. **93**, 073902-4.

Blaikie, R.J., Melville, D.O.S., Alkalsi, M.M., 2006, Super-resolution near-field lithography using planar silver lenses: A review of recent developments, Microelectronic Engineering **83**, 723–729.

Boardman, A.D., Egan, P., Velasco, L., King, N., 2005, Control of planar nonlinear guided waves and spatial solitons with a left-handed medium, J. Opt. A: Pure Appl. Opt. **7**, S57–S67.

Boardman, A.D., King, N., Velasco, L., 2005, Negative refraction in perspective, Electromagnetics **25**, 365–389.

Boardman, A.D., Velasco, L., King, N., Rapoport, Y., 2005, Ultra-narrow bright spatial solitons interacting with left-handed surfaces, J. Opt. Soc. Am. B **22**, 1443–1452.

Boyd, R.W., 1992, Nonlinear Optics, Academic Press, San Diego, CA.

Cai, W., Chettiar, U.K., Kildishev, A.V., Shalaev, V.M., 2007, Optical cloaking with non-magnetic metamaterials, Nature Photonics **1**, 224–227.

Cai, W., Genov, D.A., Shalaev, V.M., 2005, Superlens based on metal-dielectric composites, Phys. Rev. B **72**, 193101-4.

Caiazzo, M., Maci, S., Engheta, N., 2004, A metamaterial surface for compact cavity resonators, IEEE Antennas Wireless and Propagation Lett. **3**, 261–264.

Campley, R.E., Mills, D.L., 1982, Surface polaritons on uniaxial antiferromagnets, Phys. Rev. B **26**, 1280–1287.

Chen, S.-Y., Maksimchuk, A., Umstadter, D., 1998, Experimental observation of relativistic nonlinear Thomson scattering, Nature **396**, 653–655.

Chen, W., Mills, D.L., 1987a, Gap solitons and the nonlinear optical response of superlattices, Phys. Rev. Lett. **58**, 160–163.

Chen, W., Mills, D.L., 1987b, Optical response of a nonlinear dielectric film, Phys. Rev. B **35**, 524–532.

Chettiar, U.K., Kildishev, A.V., Klar, T.A., Shalaev, V.M., 2006, Negative index metamaterial combining magnetic resonators with metal films, Opt. Express **14** (17), 7872–7877.

Chettiar, U.K., Kildishev, A.V., Yuan, H.-K., Cai, W., Xiao, S., Drachev, V.P., Shalaev, V.M., 2006, Dual-band negative index metamaterial: Double-negative at 813 nm and single-negative at 772 nm, http://arxiv.org/abs/physics/0612247.

Cubukcu, E., Aydin, K., Ozbay, E., Foteinopoulou, S., Soukoulis, C.M., 2003a, Electromagnetic waves: Negative refraction by photonic crystals, Nature **423**, 604–605.

Cubukcu, E., Aydin, K., Ozbay, E., Foteinopoulou, S., Soukoulis, C.M., 2003b, Subwavelength resolution in a two-dimensional photonic-crystal-based superlens, Phys. Rev. Lett. **91**, 207401-4.

D'Aguanno, G., Mattiucci, N., Bloemer, M.J., Scalora, M., 2006, Large enhancement of second harmonic generation near the zero-n gap of a negative index Bragg grating, Phys. Rev. E **73**, 036603-4.

D'Aguanno, G., Mattiucci, N., Scalora, M., Bloemer, M.J., 2004, Bright and dark gap solitons in a negative index Fabry–Pe'rot etalon, Phys. Rev. Lett. **93**, 213902-4.

D'Aguanno, G., Mattiucci, N., Scalora, M., Bloemer, M.J., 2005, TE and TM guided modes in an air waveguide with negative-index-material cladding, Phys. Rev. E **71**, 046603-7.

Darmanyan, S.A., Neviere, M., Zakhidov, A.A., 2003, Surface modes at the interface of conventional and left-handed media, Opt. Commun. **225**, 233–240.

Darmanyan, S.A., Neviere, M., Zakhidov, A.A., 2005, Nonlinear surface waves at the interfaces of left-handed electromagnetic media, Phys. Rev. E **72**, 036615-6.

Depine, R.A., Lakhtakia, A., 2004, A new condition to identify isotropic dielectric-magnetic materials displaying negative phase velocity, Microwave and Optical Technology Letters **41**, 315–316.

Dolling, G., Enkrich, C., Wegener, M., Soukoulis, C.M., Linden, S., 2006a, Low-loss negative-index metamaterial at telecommunication wavelengths, Opt. Lett. **31**, 1800–1802.

Dolling, G., Enkrich, C., Wegener, M., Soukoulis, C.M., Linden, S., 2006b, Simultaneous negative phase and group velocity of light in a metamaterial, Science **312**, 892–894.

Dolling, G., Wegener, M., Linden, S., 2007, Realization of a three-functional-layer negative-index photonic metamaterial, Opt. Lett. **32**, 551–553.

Dolling, G., Wegener, M., Soukoulis, C.M., Linden, S., 2007, Negative-index metamaterial at 780 nm wavelength, Opt. Lett. **32**, 53–55.

Drachev, V.P., Buin, A.K., Nakotte, H., Shalaev, V.M., 2004, Size dependent $\chi(3)$ for conduction electrons in Ag nanoparticles, Nano Lett. **4**, 1535–1539.

Drachev, P., Cai, W., Chettiar, U., Yuan, H.K., Sarychev, A.K., Kildishev, A.V., Klimeck, G., Shalaev, V.M., 2006, Experimental verification of an optical negative-index material, Laser Phys. Lett. **3**, 49–55.

Durant, S., Liu, Z., Fang, N., Zhang, X., 2006, Theory of optical imaging beyond the diffraction limit with a far-field superlens, http://arxiv.org/physics/0601163.

Eggleton, B.J., Slusher, R.E., de Sterke, C.M., Krug, P.A., Sipe, J.E., 1996, Bragg grating solitons, Phys. Rev. Lett. **76**, 1627–1630.

Engheta, N., 2002, An idea for thin subwavelength cavity resonators using metamaterials with negative permittivity and permeability, IEEE Antennas and Wireless Propagation Lett. **1**, 10–13.

Engheta, N., Salandrino, A., Alu, A., 2005, Circuit elements at optical frequencies: Nanoinductors, nanocapacitors, and nanoresistors, Phys. Rev. Lett. **95**, 095504-4.

Engheta, N., Ziolkowski, R.W., 2005, A positive future for double-negative metamaterials, IEEE Transactions on Microwave Theory and Techniques **53**, 1535–1556.

Fang, N., Lee, H., Sun, C., Zhang, X., 2005, Sub-diffraction-limited optical imaging with a silver superlens, Science **308**, 534–537.

Feise, M.W., Shadrivov, I.V., Kivshar, Y.S., 2004, Tunable transmission and bistability in left-handed band-gap structures, Appl. Phys. Lett. **85**, 1451–1453.

Feise, M.W., Shadrivov, I.V., Kivshar, Y.S., 2005, Bistable diode action in left-handed periodic structures, Phys. Rev. E **71**, 037602-4.

Foteinopoulou, S., Economou, E.N., Soukoulis, C.M., 2003, Refraction in media with a negative refractive index, Phys. Rev. Lett. **90**, 107402-4.

Foteinopoulou, S., Soukoulis, C.M., 2003, Negative refraction and left-handed behavior in two-dimensional photonic crystals, Phys. Rev. B **67**, 235107-5.

Gabitov, I.R., Indik, R.A., Litchinitser, N.M., Maimistov, A.I., Shalaev, V.M., Soneson, J.E., 2006, Double-resonant optical materials with embedded metal nanostructures, J. Opt. Soc. Am. B **23**, 535–542.

Garcia, N., Nieto-Vesperinas, M., 2002, Left-handed materials do not make a perfect lens, Phys. Rev. Lett. **88**, 207403-4; Erratum: Phys. Rev. Lett. **90** (2003), 229903.

Gibbs, H.M., 1976, Differential gain and bistability using a sodium-filled Fabry–Perot interferometer, Phys. Rev. Lett. **36** (1976), 1135-4.

Gibbs, H.M., 1985, Optical Bistability, Academic Press, Orlando, FL.

Gralak, B., Enoch, S., Tayeb, G., 2000, Anomalous refractive properties of photonic crystals, J. Opt. Soc. Am. A **17**, 1012–1020.

Grigorenko, A.N., Geim, A.K., Gleeson, H.F., Zhang, Y., Firsov, A.A., Khrushchev, I.Y., Petrovic, J., 2005, Nanofabricated media with negative permeability at visible frequencies, Nature **438**, 17–20.

Hartstein, A., Burstein, E., Maradudin, A.A., Brewer, R., Wallis, R.F., 1973, Surface polaritons on semi-infinite gyromagnetic media, J. Phys. C: Solid State Phys. **6**, 1266–1276.

Hegde, R.S., Winful, H., 2005a, Optical bistability in periodic nonlinear structures containing left handed materials, Microwave and Optical Technology Letters **46**, 528–530.

Hegde, R.S., Winful, H., 2005b, Zero-n gap soliton, Opt. Lett. **30**, 1852–1854.

Houck, A.A., Brock, J.B., Chuang, I.L., 2003, Experimental observations of a left-handed material that obeys Snell's law, Phys. Rev. Lett. **90**, 137401-4.

Jacob, Z., Alekseyev, L.V., Narimanov, E., 2006, Optical Hyperlens: Far-field imaging beyond the diffraction limit, Opt. Express **14**, 8247–8256.

Jiang, H., Chen, H., Zhu, S., 2006, Localized gap-edge fields of one-dimensional photonic crystals with an ε-negative and a μ-negative defect, Phys. Rev. E **73**, 046601-5.

Joannopoulos, J.D., Meade, R.D., Winn, J.N., 1995, Photonic Crystals, Princeton University Press, Princeton.

John, S., 1987, Strong localization of photons in certain disordered dielectric superlattices, Phys. Rev. Lett. **58**, 2486–2489.

Khoo, I.C., Williams, Y., Diaz, A., Chen, K., Bossard, J., Werner, D., Graugnard, E., Summers, C.J., 2006, Liquid-crystals for optical filters, switches and tunable negative index material development, Molecular Crystal Liquid Crystal **453**, 309–319.

Kildishev, A.V., Cai, W., Chettiar, U.K., Yuan, H.-K., Sarychev, A.K., Drachev, V.P., Shalaev, V.M., 2006, Negative refractive index in optics of metal–dielectric composites, J. Opt. Soc. Am. B **23**, 423–433.

Klar, T.A., Kildishev, A.V., Drachev, V.P., Shalaev, V.M., 2006, Negative-index metamaterials: Going optical, IEEE J. of Selected Topics in Quantum Electronics **12**, 1106–1115.

Klein, M.W., Enkrich, C., Wegener, M., Linden, S., 2006, Second-harmonic generation from magnetic metamaterials, Science **313**, 502–504.

Kockaert, P., Tassin, P., Van der Sande, G., Veretennicoff, I., Tlidi, M., 2006, Negative diffraction pattern dynamics in nonlinear cavities with left-handed materials, Phys. Rev. A **74**, 033822-8.

Kosaka, H., Kawashima, T., Tomita, A., Notomi, M., Tamamura, T., Sato, T., Kawakami, S., 1998, Superprism phenomena in photonic crystals, Phys. Rev. B **58**, R10096–R10099.

Kourakis, I., Shukla, P.K., 2005, Nonlinear propagation of electromagnetic waves in negative-refraction-index composite materials, Phys. Rev. E **72**, 016626-5.

Kozyrev, A.B., Kim, H., van der Weide, D.W., 2006, Parametric amplification in left-handed transmission line media, Appl. Phys. Lett. **88**, 264101-3.

Lagarkov, A.N., Kissel, V.N., 2004, Near-perfect imaging in a focusing system based on a left-handed-material plate, Phys. Rev. Lett. **92**, 077401.

Lagarkov, A.N., Sarychev, A.K., 1996, Electromagnetic properties of composites containing elongated conducting inclusions, Phys. Rev. B **53**, 6318–6336.

Lamb, H., 1904, Proc. Lond. Math. Soc. **1**, 473–479.

Landau, L.D., Lifshitz, E.M., Pitaevskii, L.P., 1984, Electrodynamics of Continuous Media, vol. 8, second ed., Butterworth–Heinemann, Oxford.

Lapine, M., Gorkunov, M., Ringhofer, K.H., 2003, Nonlinearity of a metamaterial arising from diode insertions into resonant conductive elements, Phys. Rev. E **67**, 065601-4.

Larkin, I.A., Stockman, M.I., 2005, Imperfect perfect lens, Nano Lett. **5**, 339–343.

Lazarides, N., Tsironis, G.P., 2005, Coupled nonlinear Schrodinger field equations for electromagnetic wave propagation in nonlinear left-handed materials, Phys. Rev. E **71**, 036614.

Leonhardt, U., 2003, Notes on waves with negative phase velocity, IEEE J. of Selected Topics in Quantum Electronics **9**, 102–105.

Leonhardt, U., 2006, Optical conformal mapping, Science **312**, 1777–1780.

Leonhardt, U., Philbin, T.G., 2006, General relativity in electrical engineering, New J. Phys. **8**, 247, doi:10.1088/1367-2630/8/10/247.

Li, J., Zhou, L., Chan, C.T., Sheng, P., 2003, Photonic band gap from a stack of positive and negative index materials, Phys. Rev. Lett. **90**, 083901-4.

Lin, S.Y., Hietala, V.M., Wang, L., Jones, E.D., 1996, Highly dispersive photonic band-gap prism, Opt. Lett. **21**, 1771–1773.

Linden, S., Enkrich, C., Wegener, M., Zhou, J., Koschny, T., Soukoulis, C.M., 2004, Magnetic response of metamaterials at 100 Terahertz, Science **306**, 1351–1353.

Litchinitser, N.M., Eggleton, B.J., Patterson, D.B., 1997, Fiber Bragg gratings for dispersion compensation in transmission: Theoretical model and design criteria for nearly ideal pulse recompression, IEEE J. Lightwave Technol. **15**, 1303–1313.

Litchinitser, N.M., Gabitov, I.R., Maimistov, A.I., Shalaev, V.M., 2007, Effect of an optical negative index thin film on optical bistability, Opt. Lett. **32**, 151–153.

Litvak, A.G., Mironov, V.A., 1968, Surface waves on the separation boundary between nonlinear media, ISV. Vysch. Uch. Zav.-Radiofisika **11**, 1911–1912.

Liu, Z., Fang, N., Yen, T.-J., Zhang, X., 2003, Rapid growth of evanescent wave with a silver superlens, Appl. Phys. Lett. **83**, 5184–5186.
Lomakin, V., Fainman, Y., Urzhumov, Y., Shvets, G., 2006, Doubly negative metamaterials in the near infrared and visible regimes based on thin film nanocomposites, Opt. Express **14**, 11164–11177.
Luo, C., Johnson, S.G., Joannopoulos, J.D., Pendry, J.B., 2002, All-angle negative refraction without negative effective index, Phys. Rev. B **65**, 201104(4).
Maimistov, A.I., Gabitov, I.R., Kazantseva, E.V., 2007, Quadratic solitons in negative refractive index medium, arXiv:nlin.SI/0604015; Optics and Spectroscopy **102** (1) (2007) 104–112.
Mandelshtam, L.I., 1947, Complete Collected Works, Akad. Nauk SSSR, Moscow.
Marcuse, D., 1991, Theory of Dielectric Optical Waveguides, second ed., Academic Press, San Diego, CA.
Marklund, M., Shukla, P.K., Stenflo, L., 2006, Ultrashort solitons and kinetic effects in nonlinear metamaterials, Phys. Rev. E **73**, 037601-4.
Melville, D., Blaikie, R., 2005, Super-resolution imaging through a planar silver layer, Opt. Express **13**, 2127–2134.
Melville, D.O.S., Blaikie, R.J., Wolf, C.R., 2004, Submicron imaging with a planar silver lens, Appl. Phys. Lett. **84** (22), 4403–4405.
Merlin, R., 2004, Analytical solution of the almost-perfect-lens problem, Appl. Phys. Lett. **84**, 1290–1292.
Milton, G.W., Nicorovici, N.-A.P., 2006, On the cloaking effects associated with anomalous localized resonance, Proc. Roy. Soc. London A **462**, 3027–3059.
Nicorovici, N.A., McPhedran, R.C., Milton, G.W., 1994, Optical and dielectric properties of partially resonant composites, Phys. Rev. B (Solid State) **490**, 8479–8482.
Notomi, M., 2000, Theory of light propagation in strongly modulated photonic crystals: Refractionlike behavior in the vicinity of the photonic band gap, Phys. Rev. B **62**, 10696–10705.
O'Brien, S., McPeake, D., Ramakrishna, S.A., Pendry, J.B., 2004, Near-infrared photonic band gaps and nonlinear effects in negative magnetic metamaterials, Phys. Rev. B **69**, 241101-4.
Oktel, M.Ö., Müstecaplıoglu, Ö.E., 2004, Electromagnetically induced left-handedness in a dense gas of three-level atoms, Phys. Rev. A **70**, 053806-7.
Ozbay, E., Bulua, I., Aydina, K., Caglayana, H., Guvena, K., 2004, Physics and applications of photonic crystals, Photonics Nanostruct. Fundam. Appl. **2**, 87–95.
Pafomov, V.E., 1959, Sov. Phys. JETP **9**, 1321–1324.
Panina, L.V., Grigorenko, A.N., Makhnovskiy, D.P., 2002, Optomagnetic composite medium with conducting nanoelements, Phys. Rev. B **66**, 155411.
Parimi, P.V., Lu, W.T., Vodo, P., Sridhar, S., 2003, Imaging by flat lens using negative refraction, Nature **426**, 404.
Pendry, J.B., 2000, Negative refraction makes a perfect lens, Phys. Rev. Lett. **85**, 3966–3969.
Pendry, J.B., 2004, Negative refraction, Contemp. Phys. **45**, 191–202.
Pendry, J.B., Holden, A., Robbins, D.J., Stewart, W.J., 1999, Magnetism from conductors and enhanced nonlinear phenomena, IEEE Transactions on Microwave Theory anf Techniques **47**, 2075–2084.
Pendry, J.B., Ramakrishna, S.A., 2003, Focusing light using negative refraction, J. Phys.: Condens. Matter **15**, 6345–6364.
Pendry, J.B., Schurig, D., Smith, D.R., 2006, Controlling electromagnetic fields, Science **312**, 1780–1782.
Pocklington, H.C., 1905, Growth of a wave-group when the group velocity is negative, Nature **71**, 607–608.
Podolskiy, V.A., Alekseyev, L., Narimanov, E.E., 2005, Strongly anisotropic media: the THz perspectives of left-handed materials, J. Mod. Opt. **52**, 2343.
Podolskiy, V.A., Kuhta, N.A., Milton, G.W., 2005, Optimizing the superlens: Manipulating geometry to enhance the resolution, Appl. Phys. Lett. **87**, 231113(3).

Podolskiy, V.A., Narimanov, E.E., 2005a, Near-sighted superlens, Opt. Lett. **30**, 75–77.
Podolskiy, V.A., Narimanov, E.E., 2005b, Strongly anisotropic waveguide as a nonmagnetic left-handed system, Phys. Rev. B **71**, 201101(R).
Podolskiy, V.A., Sarychev, A.K., Narimanov, E.E., Shalaev, V.M., 2005, Resonant light interactions with plasmonic nanowire system, J. Opt. A: Pure Appl. Opt. **7**, S32–S37.
Podolskiy, V.A., Sarychev, A.K., Shalaev, V.M., 2002, Plasmon modes in metal nanowires and left-handed materials, J. of Nonlinear Opt. Physics and Materials **11**, 65.
Podolskiy, V.A., Sarychev, A.K., Shalaev, V.M., 2003, Plasmon modes and negative refraction in metal nanowire composites, Opt. Express **11**, 735.
Pokrovsky, A.L., Efros, A.L., 2003, Lens based on the use of left-handed materials, Appl. Opt. **42**, 5701–5706.
Popov, A.K., Shalaev, V.M., 2006a, Negative-index metamaterials: Second-harmonic generation, Manley–Rowe relations and parametric amplification, Appl. Phys. B **84**, 131–137.
Popov, A.K., Shalaev, V.M., 2006b, Compensating losses in negative-index metamaterials by optical parametric amplification, Opt. Lett. **31** (14), 2169–2171.
Popov, A.K., Slabko, V.V., Shalaev, V.M., 2006, Second harmonic generation in left-handed metamaterials, Laser Phys. Lett. **3**, 293–297.
Qing, De-Kui, Chen, G., 2004, Goos–Hanchen shifts at the interfaces between left- and right-handed media, Opt. Lett. **29** (8), 872–874.
Ramakrishna, S.A., 2005, Physics of negative refractive index materials, Rep. Prog. Phys. **68**, 449–521.
Ramakrishna, S., Pendry, J.B., 2003, Removal of absorption and increase in resolution in a near-field lens via optical gain, Phys. Rev. B **67**, 201101-4.
Ramakrishna, S., Pendry, J.B., Wiltshire, M.C.K., Stewart, W.J., 2003, Imaging the near field, J. Mod. Opt. **50**, 1419–1430.
Rautian, S.G., 1997, Nonlinear saturation spectroscopy of the degenerate electron gas in spherical metallic particles, JETP **85**, 451–461.
Ruppin, R., 2000, Surface polaritons of a left-handed medium, Phys. Lett. A **277**, 61–64.
Ruppin, R., 2001, Surface polaritons of a left-handed material slab, J. Phys.: Condens. Matter **13** (9), 1811–1818.
Russell, P.St.J., 1991, Bloch wave analysis of dispersion and pulse propagation in pure distributed feedback structures, J. Mod. Opt. **38**, 1599–1619.
Salandrino, A., Engheta, N., 2006, Far-field subdiffraction optical microscopy using metamaterial crystals: Theory and simulations, Phys. Rev. B **74**, 075103.
Sarychev, A.K., Shvets, G., Shalaev, V.M., 2006, Magnetic plasmon resonance, Phys. Rev. E **73**, 036609-10.
Scalora, M., D'Aguanno, G., Mattiucci, N., Akozbek, N., Bloemer, M.J., Centini, M., Sibilia, C., Bertolotti, M., 2005, Pulse propagation, dispersion, and energy in negative index materials, Phys. Rev. E **72**, 066601-8.
Scalora, M., Syrchin, M., Akozbek, N., Poliakov, E.Y., D'Aguanno, G., Mattiucci, N., Bloemer, M.J., Zheltikov, A.M., 2005, Generalized nonlinear Schrodinger equation for dispersive susceptibility and permeability: applications to negative index materials, Phys. Rev. Lett. **95**, 013902-4; Erratum: Phys. Rev. Lett. **95** (2005), 239902(E).
Schonbrun, E., Tinker, M., Park, W., Lee, J.-B., 2005, Negative refraction in a si-polymer photonic crystal membrane, IEEE Photon. Technol. Lett. **17**, 1196–1198.
Schurig, D., Mock, J.J., Justice, B.J., Cummer, S.A., Pendry, J.B., Starr, A.F., Smith, D.R., 2006, Metamaterial electromagnetic cloak at microwave frequencies, Science **314**, 977–980.
Schuster, A., 1904, An Introduction to the Theory of Optics, Edward Arnold, London.
Shadrivov, I.V., 2004, Nonlinear guided waves and symmetry breaking in left-handed waveguides, Photonics Nanostruct.: Fundam. Appl. **2**, 175–180.

Shadrivov, I.V., Kivshar, Y.S., 2005, Spatial solitons in nonlinear left-handed metamaterials, J. Opt. A: Pure Appl. Opt. **7**, S68–S72.
Shadrivov, I.V., Sukhorukov, A.A., Kivshar, Yu.S., 2003a, Guided modes in negative-refractive-index waveguides, Phys. Rev. E **67**, 057602-4.
Shadrivov, I.V., Sukhorukov, A.A., Kivshar, Y.S., Zharov, A.A., Boardman, A.D., Egan, P., 2004, Nonlinear surface waves in left-handed materials, Phys. Rev. E **69**, 016617-9.
Shadrivov, I.V., Zharov, A.A., Kivshar, Yu.S., 2003, Giant Goos–Hanchen effect at the reflection from left-handed metamaterials, Appl. Phys. Lett. **83** (13), 2713–2715.
Shadrivov, I.V., Zharov, A.A., Kivshar, Y.S., 2006, J. Opt. Soc. Am. B **23**, 529–534.
Shadrivov, I., Zharova, N., Zharov, A., Kivshar, Y., 2005, Nonlinear transmission and spatiotemporal solitons in metamaterials with negative refraction, Opt. Express **13**, 1291–1298.
Shalaev, V.M., 2007, Optical negative-index metamaterials, Nature Photonics **1**, 41–47.
Shalaev, V.M., Cai, W., Chettiar, U.K., Yuan, H., Sarychev, A.K., Drachev, V.P., Kildishev, A.V., 2005, Negative index of refraction in optical metamaterials, Opt. Lett. **30**, 3356–3358.
Shamonina, E., Kalinin, V.A., Ringhofer, K.H., Solymar, L., 2001, Imaging, compression and Poynting vector streamlines for negative permittivity materials, Electron. Lett. **37**, 1243–1244.
Shelby, R.A., Smith, D.R., Schultz, S., 2001, Experimental verification of a negative index of refraction, Science **292**, 77–79.
Shen, J.T., Platzman, P.M., 2002, Near field imaging with negative dielectric constant lenses, Appl. Phys. Lett. **80**, 3286–3288.
Shen, Y.R., 1984, The Principles of Non-Linear Optics, John Wiley & Sons, New York.
Shvets, G., 2003, Photonic approach to making a material with a negative index of refraction, Phys. Rev. B **67**, 035109-8.
Shvets, G., Urzhumov, Y., 2006, Negative index meta-materials based on two-dimensional metallic structures, J. Opt. A **8**, S122–S130.
Sivukhin, D.V., 1957, The energy of electromagnetic waves in dispersive media, Opt. Spektrosk. **3**, 308–312.
Smith, D.R., Padilla, W.J., Vier, D.C., Nemat-Nasser, S.C., Schultz, S., 2000, Composite medium with simultaneously negative permeability and permittivity, Phys. Rev. Lett. **84**, 4184–4187.
Smith, D.R., Pendry, J.B., Wiltshire, M.C.K., 2004, Metamaterials and negative refractive index, Science **305**, 788–792.
Smolyaninov, I.I., Hung, Y.J., Davis, C.C., 2006, Magnifying superlens in the visible frequency range, http://arxiv.org/physics/0610230.
Sommerfeld, A., 1909, The broadening of the waves and the wireless telegraph, Ann. Phys. (Leipzig) **28**, 665–736.
't Hooft, G.W., 2001, Comment on "Negative Refraction Makes a perfect lens", Phys. Rev. Lett. **87**, 249701-4.
Tamir, T. (Ed.), 1988, Guided-Wave Optoelectronics, Springer-Verlag, Heidelberg.
Tassin, P., Van der Sande, G., Veretenov, N., Kockaert, P., Veretennicoff, I., Tlidi, M., 2006, Three-dimensional structures in nonlinear cavities containing left-handed materials, Opt. Express **14**, 9338–9343.
Taubner, T., Korobkin, D., Urzhumov, Y., Shvets, G., Hillenbrand, R., 2006, Near-field microscopy through a SiC superlens, Science **313**, 1595.
Thommen, Q., Mandel, P., 2006, Electromagnetically induced left handedness in optically excited four-level atomic media, Phys. Rev. Lett. **96**, 053601-4.
Tretyakov, S.A., 2001, Meta-materials with wideband negative permittivity and permeability, Microwave and Optical Technology Letters **31**, 163–165.
Trutschel, U., Lederer, F., 1988, Optical response of nonlinear absorbing and saturable superlattices, J. Opt. Soc. Am. **5**, 2530–2536.
Trutschel, U., Lederer, F., Langbein, U., 1989, Transmission and reflection of transverse-magnetic-polarized optical fields at stratified nonlinear media, Phys. Rev. B **40**, 8275–8283.

Uchida, K., Kaneko, S., Omi, S., Hata, C., Tanji, H., Asahara, Y., Ikushima, A.J., Tokizaki, T., Nakamura, A., 1994, Optical nonlinearities of a high concentration of small metal particles dispersed in glass: Copper and silver particles, J. Opt. Soc. Am. B **11**, 1236–1243.
Veselago, V.G., 1968, Soviet Physics Uspekhi **10**, 509–514.
Veselago, V., Braginsky, L., Shklover, V., Hafner, Ch., 2006, Negative refraction index materials, J. of Computational and Theoretical Nanoscience **3**, 189–218.
Veselago, V.G., Narimanov, E.E., 2006, The left hand of brightness: Past, present and future of negative index materials, Nature Materials **5**, 759–762.
Von Laue, M., 1905, Die Fortpflanzung der Strahlung in dispergierenden und absorbierenden Medien, Ann. Phys. **18**, 523–566.
Wangberg, R., Elser, J., Narimanov, E.E., Podolskiy, V.A., 2006, Nonmagnetic nanocomposites for optical and infrared negative-refractive-index media, J. Opt. Soc. Am. B **23**, 498–505.
Ward, A.J., Pendry, J.B., 1996, Refraction and geometry in Maxwell's equations, J. Mod. Opt. **43**, 773–793.
Wegener, M., 2005, Extreme Nonlinear Optics, Springer-Verlag, Berlin, Heidelberg, Germany.
Williams, J.M., 2001, Some problems with negative refraction, Phys. Rev. Lett. **87**, 249703-4.
Winful, H.G., Marburger, J.H., Garmire, E., 1979, Theory of bistability in nonlinear distributed feedback structures, Appl. Phys. Lett. **35**, 376–378.
Yablonovitch, E., 1987, Inhibited spontaneous emission in solid-state physics and electronics, Phys. Rev. Lett. **58**, 2059–2062.
Ye, Z., 2003, Optical transmission and reflection of perfect lenses by left handed materials, Phys. Rev. B **67**, 193106.
Zhang, S., Fan, W., Panoiu, N.C., Malloy, K.J., Osgood, R.M., Brueck, S.R.J., 2005, Demonstration of near-infrared negative-index materials, Phys. Rev. Lett. **95**, 137404-4.
Zhang, S., Fan, W., Panoiu, N.C., Malloy, K.J., Osgood, R.M., Brueck, S.R.J., 2006, Optical negative-index bulk metamaterials consisting of 2D perforated metal-dielectric stacks, Opt. Express **14**, 6778–6787.
Zharov, A.A., Shadrivov, I.V., Kivshar, Yu.S., 2003, Nonlinear properties of left-handed metamaterials, Phys. Rev. Lett. **91**, 037401-4.
Zharov, A.A., Zharova, N.A., Shadrivov, I.V., Kivshar, Yu.S., 2005, Subwavelength imaging with opaque nonlinear left-handed lenses, Appl. Phys. Lett. **87**, 091104-3.
Zhou, J., Zhang, L., Tuttle, G., Koschny, T., Soukoulis, C.M., 2006, Negative index materials using simple short wire pairs, Phys. Rev. B **73**, 041101-4.
Ziolkowski, R.W., 2006, Ultrathin, metamaterial-based laser cavities, J. Opt. Soc. Am. B **23**, 451–460.
Ziolkowski, R.W., Hayman, E., 2001, Wave propagation in media having negative permittivity and permeability, Phys. Rev. E **64**, 056625-15.